Tectonics®

RESEARCH ARTICLE
10.1029/2023TC007758

Surface Rupturing Earthquakes of the Greater Caucasus Frontal Thrusts, Azerbaijan

Ian Pierce[1], Ibrahim Guliyev[2], Gurban Yetirmishli[3], Rauf Muradov[3], Sabina Kazimova[3], Rashid Javanshir[1,2], Gregory P. De Pascale[4], Ben Johnson[1], Neill Marshall[1], Richard Walker[1], and Paul Wordsworth[1]

[1]University of Oxford, Oxford, UK, [2]Azerbaijan National Academy of Science, Baku, Azerbaijan, [3]Republican Seismic Survey Center of Azerbaijan National Academy of Science, Baku, Azerbaijan, [4]Institute of Earth Science, University of Iceland, Reykjavík, Iceland

Abstract Here we present the results of the first paleoseismic study of the Kura fold-thrust belt in Azerbaijan based on field mapping, fault trenching, and Quaternary dating. Convergence at rates of ∼10 mm/yr between the Arabian and Eurasian Plates is largely accommodated by the Kura fold-thrust belt which stretches between central Azerbaijan and Georgia along the southern front of the Greater Caucasus (45–48°E). Although destructive historic earthquakes are known here, little is known about the active faults responsible for these earthquakes. A paleoseismic trench was excavated across a 2-m-high fault scarp near Agsu revealing evidence of two surface rupturing earthquakes. Radiocarbon dating of the faulted sediments limits the earthquake timing to AD 1713–1895 and AD 1872–2003. Allowing for uncertainties in dating, the two events likely correspond to historical destructive $M \sim 7$ earthquakes near Shamakhi, Azerbaijan in AD 1668 and 1902. A second trench 60 km west of Agsu was excavated near Goychay also revealing evidence of at least one event that occurred 334–118 BC. Holocene shortening and dip-slip rates for the Kura fold-thrust belt are ∼8.0 and 8.5 mm/yr, respectively, based on an uplifted strath terrace west of Agsu. The only known historical devastating ($M > \sim 7$) earthquakes in the Kura region, west of Shamakhi, occurred in 1139 and possibly 1668. The lack of reported historical ruptures from the past 4–8 centuries in the Kura, in contrast with the numerous recorded destructive earthquakes in Shamakhi, suggests that the Kura fold-thrust belt may have accumulated sufficient strain to produce a $M > 7.7$ earthquake.

Plain Language Summary The Greater Caucasus Mountains stretching between the Black and Caspian Seas are a result of the northward subduction of the Arabian plate beneath Eurasia. For the last 1.5 million years, most of this plate motion has been accommodated by the Kura fold-thrust belt in Azerbaijan & eastern Georgia. This plate motion produces infrequent but damaging large earthquakes. Here a geologic mapping and paleoseismic trenching investigation revealed evidence for large earthquakes in the eastern part of the Kura fold-thrust belt of Azerbaijan. These earthquakes likely correspond to known historical earthquakes in 1668 and 1902, as well as one or more earlier, undocumented earthquakes. A lack of historical earthquakes to the west of this study area suggest that the rest of the Kura fold-thrust belt may produce less frequent, but stronger earthquakes along this plate boundary.

Key Points:

- Two paleoseismic trenches near Goychay and Agsu, Azerbaijan provide evidence of at least three surface rupturing events
- Events occurred 334–118 BC, AD 1713–1895, and AD 1872–2003. The latter two may correspond to historical earthquakes in 1668 and 1902
- Maximum Holocene shortening and dip-slip rates of the frontal thrust sheet in the eastern Kura fold-thrust belt are 8 and 8.5 mm/yr, respectively

Correspondence to:
I. Pierce,
ian@nevada.unr.edu

Citation:
Pierce, I., Guliyev, I., Yetirmishli, G., Muradov, R., Kazimova, S., Javanshir, R., et al. (2024). Surface rupturing earthquakes of the Greater Caucasus frontal thrusts, Azerbaijan. *Tectonics*, *43*, e2023TC007758. https://doi.org/10.1029/2023TC007758

Received 11 JAN 2023
Accepted 22 FEB 2024

Author Contribution:
Investigation: Gregory P. De Pascale
Writing – review & editing: Gregory P. De Pascale

1. Introduction

The Greater Caucasus Mountains extend for 900 km between the Black and Caspian Seas (Figure 1) and were uplifted since ∼5 Ma due to the northeast-directed subduction of the Arabian plate beneath the Eurasian plate (Avdeev & Niemi, 2011; Cowgill et al., 2016; Forte et al., 2015; Gunnels et al., 2021; Jackson et al., 2002; Kangarli et al., 2018; McKenzie, 1972; Mumladze et al., 2015; Philip et al., 1989). High resolution 3-D tomographic models and relocated earthquake hypocenters suggest that this subduction is active and ongoing beneath the eastern part of the Greater Caucasus in Azerbaijan (Gunnels et al., 2021). This subduction is largely accommodated by the north-dipping Main Caucasus Thrust Fault, a major plate boundary fault, which since ∼1.5 Ma has been surficially expressed in the foreland Kura fold-thrust belt (Forte et al., 2013).

The Kura fold-thrust belt extends roughly west-east for ∼275 km from near Tbilisi, Georgia to near Shamakhi, Azerbaijan (Figure 1a). The belt forms an imbricate pattern that varies along strike with between one and four thrust sheets reaching the surface. An average shortening rate of 6.7–13.6 mm/yr for the last ∼1.5 Ma has been estimated using the restoration of balanced cross sections across the Kura fold-thrust belt (Forte et al., 2013;

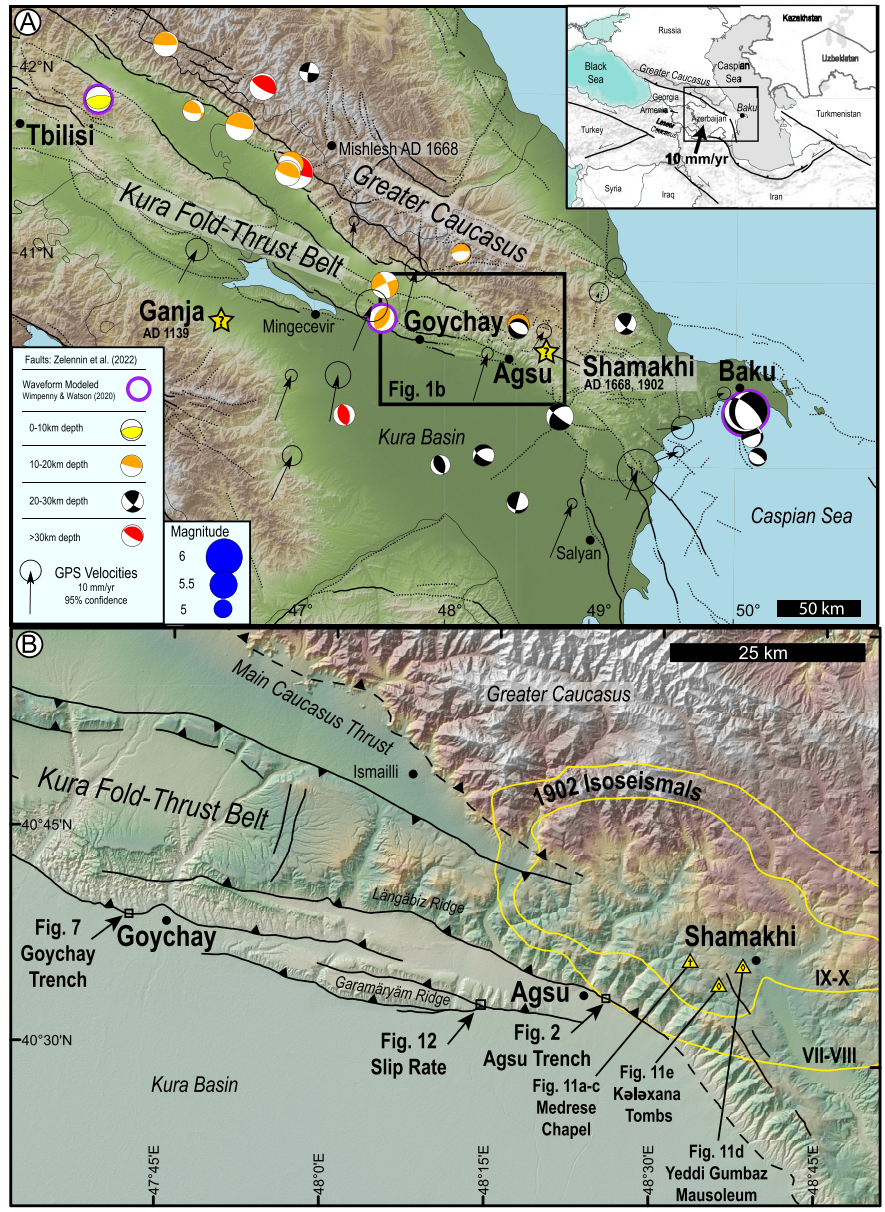

Figure 1. Overview map of (a) Azerbaijan showing GPS velocities relative to stable Eurasia (Kadirov et al., 2012), faults from the Active Faults of Eurasia Database (Zelenin et al., 2022), and focal mechanisms of earthquakes from the gCMT (Dziewonski et al., 1981; Ekström et al., 2012) and gWFM (Wimpenny & Watson, 2020) catalogs with ISC-EHB hypocenters from 1976-present (Engdahl et al., 1998, 2020; International Seismological Centre, 2022; Weston et al., 2018). (b) Is the eastern part of the Kura fold-thrust belt showing major faults (our mapping, black lines, dashed where approximate) and figure locations including trench sites, slip rate measurement site, and archeological monuments. The Kura fold-thrust belt has accommodated >80% of the shortening between the Lesser Caucasus and Greater Caucasus since ~1.5 Ma, at an average rate of ~7–14 mm/yr (Forte et al., 2013). Yellow lines are MMI scale isoseismals of the 1902 Shamakhi earthquake adapted from the original intensity scale developed by Weber (1903). Inset simplifies major regional tectonic faults and representative GPS velocity relative to stable Eurasia.

Kangarli et al., 2018; Mosar et al., 2010). Modeling of GPS data shows that shortening rates across the front of the Greater Caucasus decrease westward from ~10 mm/yr near the Caspian Sea to ~4 mm/yr near Tbilisi (Kadirov et al., 2012; Reilinger et al., 2006; Yetirmishli et al., 2022).

Previous neotectonic research in the Greater Caucasus and Kura fold-thrust belt primarily focused on the structural geometry, kinematics, regional tectonics, and the identification of active structures (Alania et al., 2017; Allen

et al., 2003; Avdeev & Niemi, 2011; Cowgill et al., 2016; Forte, 2012; Forte et al., 2010, 2013, 2014, 2015; Sokhadze et al., 2018; Sukhishvili et al., 2021; Tibaldi et al., 2017; Trexler et al., 2020; Trifonov, 1978). In contrast, few studies have utilized paleoseismic trenching to examine faults in the Greater Caucasus (Ovsyuchenko et al., 2014; Rogozhin et al., 2004). The only published paleoseismic trenching study we are aware of that specifically focuses on the frontal thrust belt investigated a low-slip-rate structure to the west of Tbilisi in Georgia (Stahl et al., 2022).

The largest instrumental-period earthquakes in the Caucasus region are the 1991 M_s 7.0 Racha, Georgia (Triep et al., 1995) and the 1988 M_s 6.9 Spitak, Armenia (Philip et al., 1992) events. However, neither of these earthquakes occurred in the Kura fold-thrust belt. Historical destructive earthquakes in the Kura region include the AD 1139 Ganja earthquake and the 1668 and 1828–1902 Shamakhi earthquakes (Ismail-Zadeh et al., 2020). The 1668 and 1828–1902 events all occurred near Shamakhi (1902 isoseismals are indicated on Figure 1b), in the easternmost part of the Kura fold-thrust belt. Jackson and Ambraseys (1997) suggest that known historical seismicity over the past 400 years accounts for only 25% of the geologic shortening in the Caucasus. This discrepancy raises significant uncertainty regarding the seismogenic potential of faults in the region, as it is unclear whether the absence of historical seismicity to the west of Shamakhi is due to (a) lapses in historical records (due to sparse populations, lack of record keeping, or other reasons), (b) aseismic deformation (e.g., fault creep), or (c) unreleased moment accumulating in the Kura fold-thrust system.

Therefore, investigating the paleoseismic history of faults in the Kura fold-thrust belt is crucial for understanding not only the seismic potential and behavior of these faults, but also understanding the mechanics of continental subduction in this young orogen. In this paper, we present the first paleoseismic trench investigations and a slip rate estimate from the Kura fold-thrust belt in Azerbaijan. We also document damage to cultural monuments that resulted from the 1902 Shamakhi earthquake. We then discuss the significance of these findings and place them in the context of the historical earthquake catalog.

2. Methods

2.1. Fault Mapping, Photogrammetry, and Paleoseismic Trenching

Faults were remotely mapped using Google Earth and elevation models constructed from Pleiades stereo satellite imagery Pierce & Walker, 2023 (https://doi.org/10.5069/G9RJ4GPJ), prior to field reconnaissance mapping from 2021 to 2023. Reconnaissance mapping consisted of driving and/or walking portions of all of the faults identified in Figure 1b. Key study sites were then surveyed in high detail with photogrammetry using images captured with a Teokit-equipped DJI Phantom 4 Pro v2 drone. The Teokit is a dGPS used for acquiring precise photo locations that are then PPK corrected to an Emlid Reach RS2 dGPS base station (Zhang et al., 2019). The resulting photographs were processed using Agisoft Metashape software into DEMs and Orthomosaics, with resolutions of 6–10 and 3–5 cm/pixel, respectively (see Data Availability statement for access). Two paleoseismic trenches across mapped fault traces were excavated, cleaned, gridded, and logged. As a base for logging, 3D Structure-from-Motion (SfM) models of the trenches were constructed using Agisoft Metashape software with photographs captured with a Samsung Galaxy S20 Ultra (2022) and a Pixel 7 Pro (2023). The SfM models were accurately rectified, oriented, and scaled in real world units using reference points extracted from iPad-lidar scans of the trench walls, prior to construction and export of the 2D orthohoto mosaic images (Pierce & Koehler, 2023). The results of this process are 2D images of the trench wall with cm-scale geometric errors (Pierce, 2022, 2023). Logging was then conducted on these 2D images using an iPad. Units and faults were divided and described following standard paleoseismic methods (McCalpin, 2009), including sedimentary facies, cross-cutting relations, and development of soils. Radiocarbon samples of charcoal, plant material, bone, and soil were logged on the trench logs, sampled, processed and then analyzed at the Beta Analytic laboratory in Miami, Florida, and calibrated using OxCal v4.4 (Bronk Ramsey, 1995) with the IntCal20 calibration curve. These calibrated Ages were then plotted on the trench logs for age constraints of the different units and processing details are listed in Table 1.

3. Results

3.1. Field Reconnaissance

Our field reconnaissance focused on mapping evidence of active faulting along the easternmost 65 km of the Kura fold-thrust belt from near Goychay to Agsu (Figure 1). This section of the thrust-belt consists of two primary

Table 1
Radiocarbon Sample Data

Sample name	Location	Unit	Lat. (°)	Lon. (°)	Sample material[a]	Radiocarbon age (BP)	Calibrated[b] age (AD or BC if noted)	OxCal[b] v4.4 modeled age (AD, 95.4%)	Percent modern carbon (pMC)	δ13C (‰)	δ18O (‰)
R1	Agsu T1	U4	40.572	48.427	Charcoal	−20 ± 30	1954–1957 (60.9%) 1886–1913 (31.0%) 1707–1718 (2.4%) 1825–1832 (1.2%)	1811–1917	100.25 ± 0.37	−27.0	-
R5	Agsu T1	U4	40.572	48.427	Plant material	−2,080 ± 30	1978–1979 (89.3%) 1961 (6.1%)	-	129.55 ± 0.48	−24.8	-
R6	Agsu T1	U4	40.572	48.427	Charcoal	190 ± 30	1724–1812 (52.0%) 1648–1695 (21.8%) 1916–>1950(17.8%) 1838–1878 (3.8%)	1739–1948	97.66 ± 0.36	−24.9	-
R7	Agsu T1	U5	40.572	48.427	Plant material	−770 ± 30	1996–2000 (92.9%) 1956–1957 (2.5%)	-	110.06 ± 0.41	−28.0	-
R10	Agsu T1	U2	40.572	48.427	Plant Material	−3,410 ± 30	1967–1971 (93.2%) 1962 (2.2%)	-	152.88 ± 0.57	−25.8	-
R11	Agsu T1	U2	40.572	48.427	Plant Material	1240 ± 30	758–880 (55.8%) 679–746 (39.6%)	695–887	85.7 ± 0.32	−26.3	-
R18	Agsu T1	U5	40.572	48.427	Plastic candy wrapper	-	-	1985–2006	-	-	-
R24	Agsu T1	U2	40.572	48.427	Charcoal	70 ± 30	1810–1919 (68.7%) 1692–1727 (26.7%)	1683–1853	99.13 ± 0.37	−23.5	-
R25	Agsu T1	U2	40.572	48.427	Organic Sediment[c]	1160 ± 30	820–978 (83.9%) 772–790 (10.2%) 804–810 (1.3%)	774–979	86.55 ± 0.32	-	-
R26	Agsu T1	U1	40.572	48.427	Organic Sediment[c]	940 ± 30	1028–1172 (95.4%)	1028–1171	88.96 ± 0.33	−26.2	-
R29	Agsu T1	U1	40.572	48.427	Charcoal	120 ± 30	1799–1940 (67.2%) 1680–1740 (25.8%) 1752–1764 (2.4%)	1669–1859	98.52 ± 0.37	−26.3	-
R31	Agsu T1	U3	40.572	48.427	Charcoal	690 ± 30	1272–1317 (65.5%) 1360–1388 (29.9%)	1271–1389	91.77 ± 0.34	−25.4	-
R33	Agsu T1	W2	40.572	48.427	Plant Material	−150 ± 30	1954–1956 (95.4%)	-	101.88 ± 0.38	−29.0	-
R35	Agsu T1	W2	40.572	48.427	Charcoal	160 ± 30	1719–1786 (31.6%) 1906–>1950(19.4%) 1832–1892 (17.9%) 1664–1708 (16.7%) 1792–1819 (9.8%)	1741–1948	98.03 ± 0.37	−25.6	-
R37	Agsu T1	U2	40.572	48.427	Charcoal	180 ± 30	1722–1814 (49.9%) 1656–1698 (19.2%) 1910–>1950(19.0%) 1836–1880 (7.3%)	1650–1810	97.78 ± 0.37	−23.6	-
WG1	Water gap	-	40.559	48.236	Shell[d]	6,040 ± 30	5026–4842 BC (95.4%)	-	47.15 ± 0.18	−7.8	−2.23
GOY2	Goychay T1	U1	40.651	47.697	Charcoal	2,750 ± 30	981–948 BC (7.8%) 940–817 BC (87.7%)	966–811 BC	71.01 ± 0.27	-	-

Table 1
Continued

Sample name	Location	Unit	Lat. (°)	Lon. (°)	Sample material[a]	Radiocarbon age (BP)	Calibrated[b] age (AD or BC if noted)	OxCal[b] v4.4 modeled age (AD, 95.4%)	Percent modern carbon (pMC)	δ13C (‰)	δ18O (‰)
GOY3	Goychay T1	U5	40.651	47.697	Charcoal	2,140 ± 30	351-293 BC (19.0%) 209–52 BC (76.5%)	203–53 BC	76.61 ± 0.29	−19.3	-
GOY5	Goychay T1	U5	40.651	47.697	Bone[e]	2,090 ± 30	196–185 BC (1.3%) 179–38 BC (91.4%) 13 BC–AD 4 (2.7%)	173–42 BC	77.09 ± 0.29	−18.3	-
GOY6	Goychay T1	U1	40.651	47.697	Charcoal	2,130 ± 30	346–316 BC (10.9%) 205–51 BC (84.6%)	356–137 BC	76.71 ± 0.29	−23.9	-
GOY7	Goychay T1	U7	40.651	47.697	Charcoal	2,000 ± 30	51 BC–AD 84 (91.0%) AD 96–116 (4.4%)	52 BC–AD 79	77.96 ± 0.29	−21.7	-
GOY8	Goychay T1	U5	40.651	47.697	Charcoal	2,100 ± 30	334–331 BC (0.5%) 198–42 BC (95.0%)	176–44 BC	77.00 ± 0.29	−22.5	-
GOY9	Goychay T1	U7	40.651	47.697	Charcoal	2,030 ± 30	147–140 BC (0.6%) 108BC–AD 69(94.8%)	91 BC–AD 61	77.67 ± 0.29	−22.1	-
GOY10	Goychay T1	U2	40.651	47.697	Organic Sediment[c]	2,470 ± 30	766–465 BC (93.4%) 436–422 BC (2.1%)	766–422 BC	73.53 ± 0.27	−25.3	-

[a]All samples pretreated with acid/alkali/acid washes unless otherwise noted. [b]All calibrations conducted with OxCal v4.4 using the IntCal 20 curve. [c]Acid wash pretreatment only. [d]Acid etch pretreatment only. [e]Collagen extraction with alkali.

thrust sheets that is each surficially expressed by several faults. The more northerly sheet forms the Längäiz ridge, which is a relay ramp where the surficial faulting steps near Goychay (Forte et al., 2013). The southerly sheet begins to the east of Goychay and increases in relief eastwards as it forms a large anticline (the Garamäyäm ridge) before tapering and finally disappearing just south of Agsu. Near the center of the Garamäyäm ridge the southerly sheet is split into two thrusts, which merge eastward. The field surveys presented in the following sections of this manuscript (Figure 1b) provide evidence of displaced Holocene sediments, fault scarps, and uplifted youthful geomorphic surfaces at the fronts of each of these two primary thrusts, which demonstrates that each of these thrusts has been active in the Holocene and periodically ruptures to the ground surface during large earthquakes.

3.2. Paleoseismic Trench Near Agsu

3.2.1. Description of Agsu Trench Site

The Kura thrust immediately adjacent to Agsu follows the rangefront of the Greater Caucasus. Here the active fault forms a ∼50-m-high back-tilted (to the northeast) uplifted bench along the rangefront, with a clear fold in the crest of the uplifted surface (Figure 2). Approximately 2.5 km east of Agsu is a small alluvial valley where a stream has incised through this bench, cutting perpendicularly to the fault trace (Figures 2 and 3). This valley contains two low incised terraces, a lower T1 terrace and a 1-m-higher T2 terrace. The two terrace treads are smooth, relatively flat, and continuously traceable upstream from the valley mouth for ∼300 m (Figure 3a). At the valley mouth, both terraces are displaced, with fault scarps that are ∼2 m high. On the western margin of the valley a small stream has sharply incised into the T1 terrace. The drone-derived hillshade image shows evidence of anthropogenic modification of the scarp in the T2 terrace, but both sides of the fault in the T1 terrace appear to be unmodified and correlative. A paleoseismic trench was excavated across the 2-m-high scarp cutting across the T1 terrace in this alluvial valley (40.572°N, 48.427°E).

3.2.2. Description of Agsu Trench Exposure

The Agsu trench exposure was 22-m-long and 5-m-deep (Figure 4). The eastern wall of the trench was carefully logged and photographed. The trench revealed a series of clays, alluvium, and colluvium that are cut and deformed by a low angle fault (labeled F0) that splays up-dip (labeled F1-F4). The lowest unit in the trench, U1, is a colluvial deposit that consists of poorly sorted rounded cobbles and gravels in a fine grained silty/sandy matrix.

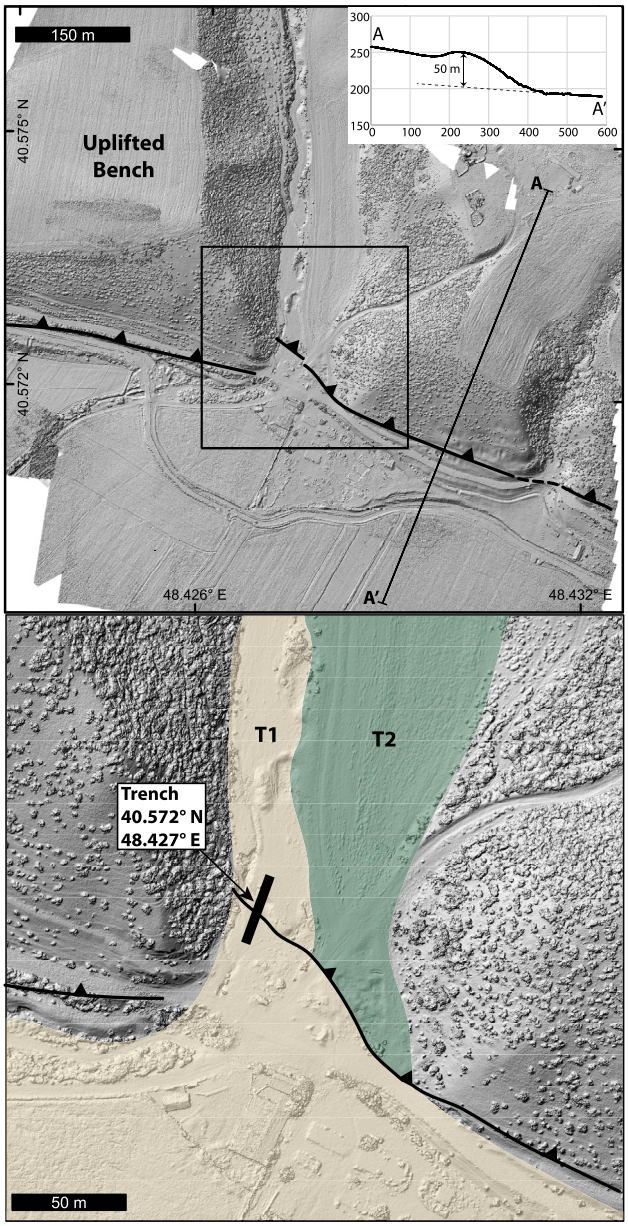

Figure 2. Hillshade image of photogrammetry-derived DEM of the trench site east of Agsu. Inset topographic profile shows characteristic folding of the 50-m-high uplifted bench along the rangefront here. Lower panel shows T1 and T2 terraces within the small alluvial valley.

Onlapping onto U1 is U2, a south-thickening sequence of interbedded, well-sorted, grain-supported fluvial sands, gravels, and rounded cobbles. We mark in gray the area where U2 onlaps onto U1, which consists of fine grained sediments that are possibly a paleosol. At the top of U2 is a ~40-cm-thick fine grained, light colored paleosol, that is readily traced across the southerly half of the trench. Above U1 in the hanging wall is U3, a 1.5-m-thick finely laminated, massive appearing clay that dries into prismatic blocks, and is highly sheared near the fault zone. Above U3 is U4, a sequence of clays, silts and sands with fine laminations. Units U4 and U5 are only present in the hangingwall. Above U4 is U5, a series of laminated silts and sands with a thin layer of cobbles, and scattered modern plastic garbage in the upper 20–30 cm. Above U2 is a poorly sorted colluvial unit, W1, composed of rounded small boulders, cobbles, and gravels in a fine grained matrix. At the top of W1 is a ~20-cm-thick, light-colored fine-grained paleosol. W1 is thickest directly below the fault scarp and tapers away from the scarp to the south. Above W1 is W2. W2 is another colluvial unit, composed of angular blocks of clay in a fine grained matrix with very few scattered pebbles.

A sub-horizontal fault (fault F0) cuts across the trench exposure and splays into 4 sub-faults in the hanging wall (faults F1 to F4). Fault F4 forms a shear zone within U3. Faults F3 and F2 bound a shear zone composed of materials from U1 and are well marked by alignments of cobbles and pebbles. Fault F1 displaces part of the soil capping U2. Units U1, U2, U3, and U4 are clearly folded in the hanging wall of the trench, while U2 is largely undeformed in the footwall.

3.2.3. Agsu Trench Event History

The stratigraphy on the southern half of the trench provides evidence of two rupturing events, clearly demarcated by the two distinct colluvial wedges (W1 & W2) resting upon undeformed fluvial sediments (U2) (Figure 4). Figure 5 provides a backslip event reconstruction model. The older, penultimate event (E1) produced the W1 colluvial wedge composed of unsorted gravels and cobbles that bury the paleosol capping the lower U2 fluvial sediments. This W1 wedge then developed a thin, fine-grained soil on its top. The younger, most recent event (E2) produced another colluvial wedge (W2), but composed of angular blocks of clay sourced from U3. This W2 wedge buried the thin soil capping the W1 penultimate wedge. The difference in materials between the two wedges is very distinct.

The penultimate E1 event ruptured the F0, F1, and F2 faults through the U1 colluvial deposit and the top of the U2 alluvial deposit at the bottom of the north-half of the trench along a sub-horizontal fault plane (Figure 5). The splaying of F0 into F1 and F2 created an abrupt fold in part of U2 and the U1 colluvial deposit, which then collapsed forming the E1 wedge.

The massive clay unit U3's deposition predates the E1 event and may have been deposited behind a fold in the U1 colluvial unit that formed during an earlier event on a different fault strand, though the trench does not expose this fault strand and this interpretation is speculative. In this interpretation, U3 would have both capped and laterally abutted U1 prior to the E1 rupture (Figure 5). Then, during the E1 rupture, the U1 unit was brought into the surficial fault zone along the nearly flat F0 fault. We speculate that F0 may be so flat in this exposure in part because the trench is slightly oblique to the fault, and as well that the U3 clay unit is much stronger than the U1 colluvial unit, so the fault exploited this rheological difference. The U3 unit, both capping and laterally abutting U1, was not brought into the surficial fault zone until more slip accumulated during the later E2 event. Following the E1 event, the clays and silts of U4 were then deposited on top of U3 on the hanging wall, behind the fold that formed during the E1 rupture. A minimum of 6.6 m of displacement can be estimated for E1 by backslipping U1 along faults F1 and F2.

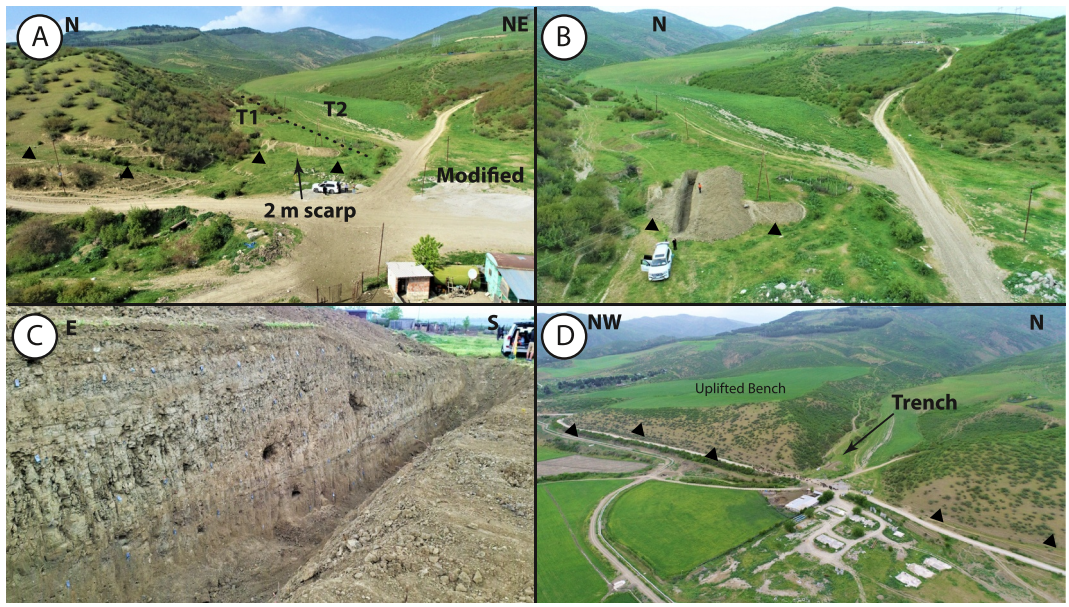

Figure 3. Aerial photographs of the trench site before (a) and after (b) trench excavation, highlighting the 2-m-high scarp and small alluvial valley. (c) Shows the excavated trench. (d) Shows the uplifted folded bench along the rangefront.

The more recent event, E2, again ruptured the F0 fault, and also ruptured the F3 fault along the base of the U3 clay, folding units U3 and U4 into a sharp fold-scarp, and again creating a colluvial wedge, W2. U5, like U4, represents growth strata deposited behind this fold on the hanging wall. A minimum of 3.5 m of displacement is required to thrust U3 over the crest of the fold in U1. As units U1 and U3 are both highly sheared in the fault zone, there is

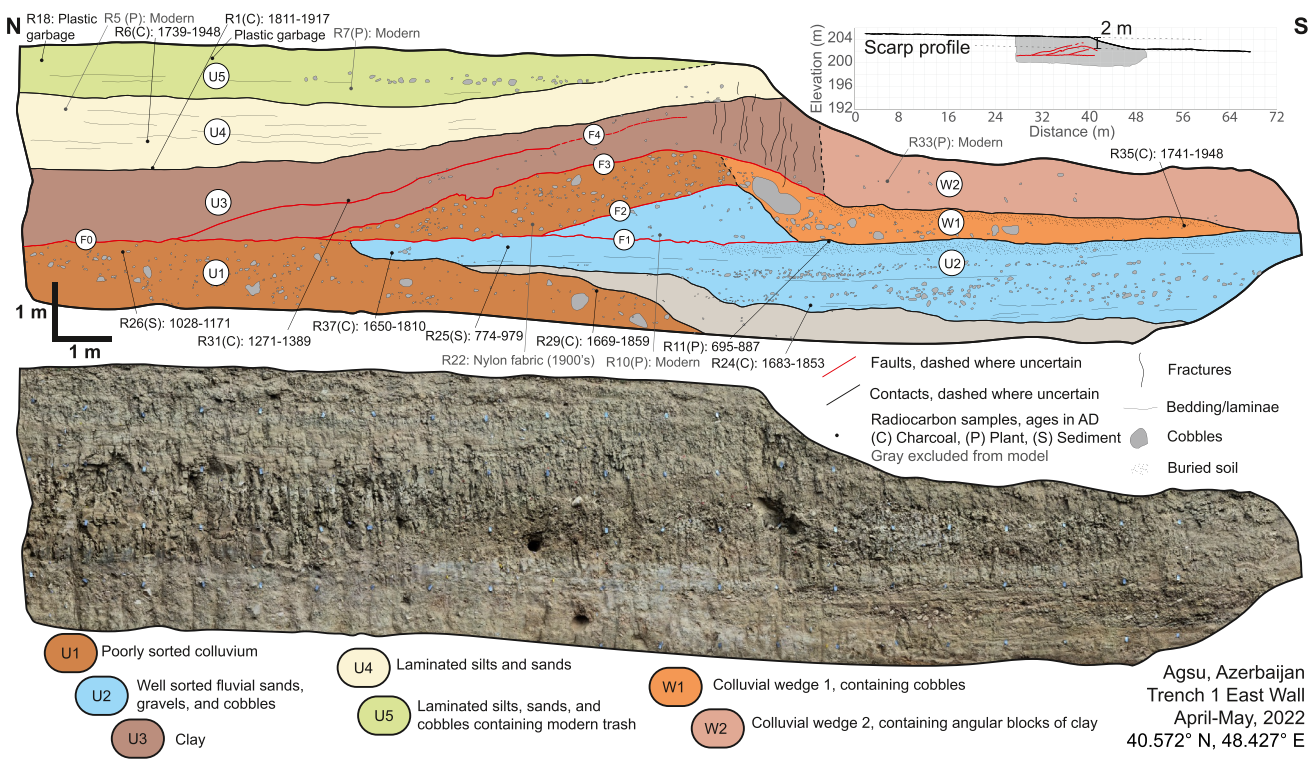

Figure 4. Trench log (upper) and photomosaic (lower) of the east wall of the Agsu trench. Inset shows position of trench within fault scarp profile. Ages listed are modeled ages as described in text. We interpret evidence of two events primarily based on the colluvial wedge stratigraphy on the footwall (W1 and W2).

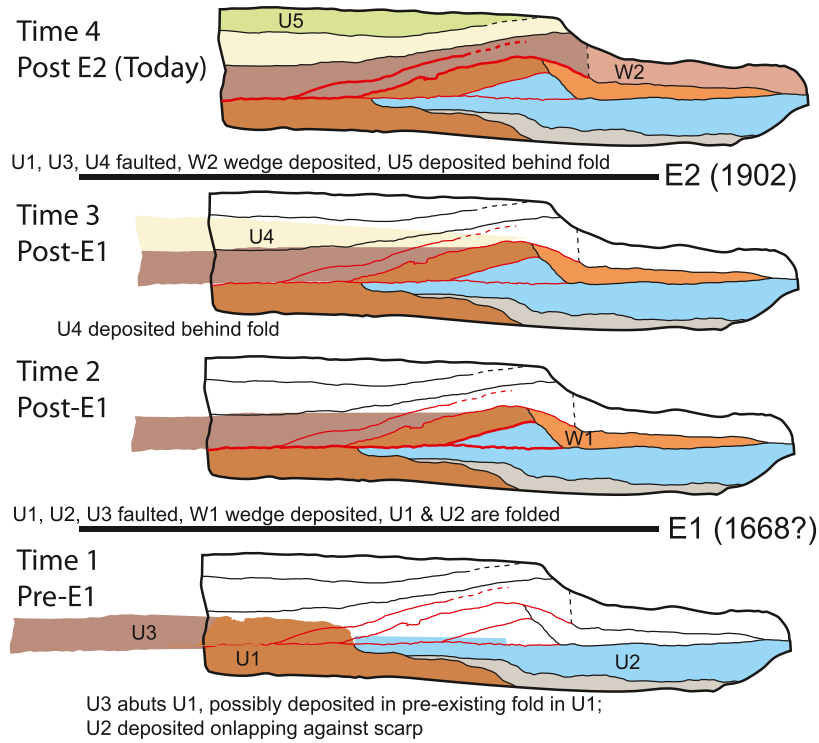

Figure 5. Backslip reconstruction of the Agsu trench. Colors and symbols are the same as in Figure 4. The most clear event evidence is the colluvial wedge stratigraphy (W1 & W2) on the footwall. Progressive folding and faulting produce growth strata on both the hanging- and foot-walls of the low angle thrust fault.

high uncertainty in these offset measurements. Taken together, the trench stratigraphy and reconstruction (Figure 5) show how shallow folding during surface rupturing earthquakes can build growth strata on both the hanging- and foot-walls of a thrust fault. This result demonstrates that scarp diffusion modeling in the absence of subsurface data (e.g., Andrews & Hanks, 1985) should not be blindly applied to estimate the formation age of thrust fault scarps.

3.2.4. Agsu ^{14}C Geochronology

The 14 radiocarbon sample locations from the Agsu trench are plotted on Figure 4, and the results are listed in Table 1. Four samples: R5, R7, R10, and R33 are all plant materials that yielded modern ages, so it is likely we inadvertanetly sampled modern plant roots, misidentifying them for detrital plant fragments, and thus we exclude them from further analysis. Sample R18 was a late 1990s vintage plastic candy wrapper, so is assumed to be from AD 1995 ± 5, and is used as an upper limit of the stratigraphic model. Samples R25 and R26 are both bulk sediment carbon samples, which can be less reliable than detrital charcoal as their resulting ages can contain large scatter (on the order of thousands of years) in samples taken from a single layer (e.g., Grützner et al., 2016). Sample R22, from within the fault zone (Unit U1), is a large piece of nylon fabric. Nylon was invented in the mid 1900s so this material must have been brought down to this level by a burrowing animal, as other samples from Unit 1 are medieval in age (R26: 1028–1171, R29: 1669–1859). Both the clear stratigraphy in the exposure and the lack of other modern materials at lower depths, compared to the concentrated amounts of plastics in the uppermost layer preclude reworking of the entire exposure. The remaining ages were placed into an OxCal sequence model (Figure 6), and the results provide limits on the timing of the two surface rupturing events: E1 occurred from AD 1713–1895, and E2 occurred from AD 1872–2003 (95.4% confidence intervals).

10.1029/2023TC007758

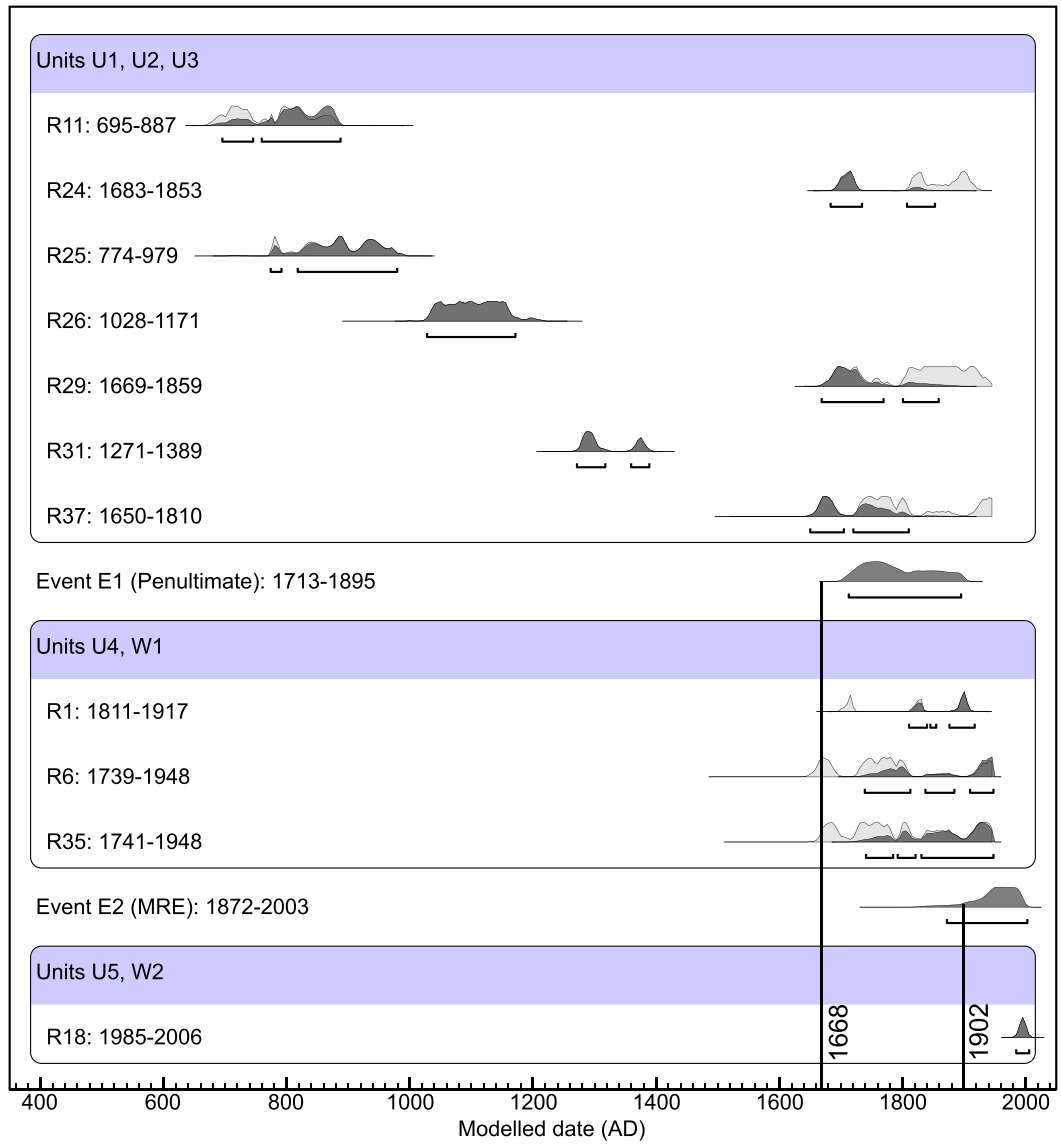

Figure 6. OxCal model of radiocarbon samples and event timing from the Agsu trench. The timing of the 1668 and 1902 historical earthquakes are plotted for reference. Event horizons for E1 and E2 are AD 1713–1895 and AD 1872–2003, respectively. Dark gray PDF's are the sequence modeled results, while light gray are the full calibrated age ranges.

3.3. Paleoseismic Trench Near Goychay

3.3.1. Description of Goychay Trench Site

In Goychay, 55 km to the west of Agsu, the Kura thrust cuts across the Goy River forming a suite of uplifted river terraces and intensely folded Pleistocene sediments. Upstream from its intersection with the fault, the Goy River forms a broad river valley with a very thin (<50-cm-thick in places) cobble strath capping a vertical walled bedrock river canyon channel. The bedrock is comprised of early Pleistocene sediments with steeply dipping beds (Forte et al., 2013). In Goychay, this bedrock channel and thin strath terraces immediately disappear and the river forms a deep cobble/gravel channel paired with cobble/gravel fill terraces. We interpret this change to be a result of the main thrust fault. A massive concrete flood control structure and extensive excavations and levies at the exact location of the fault crossing hides the fault itself, however this change in river terrace morphology, from thin straths to cobble fill terraces is stark and dramatic.

10.1029/2023TC007758

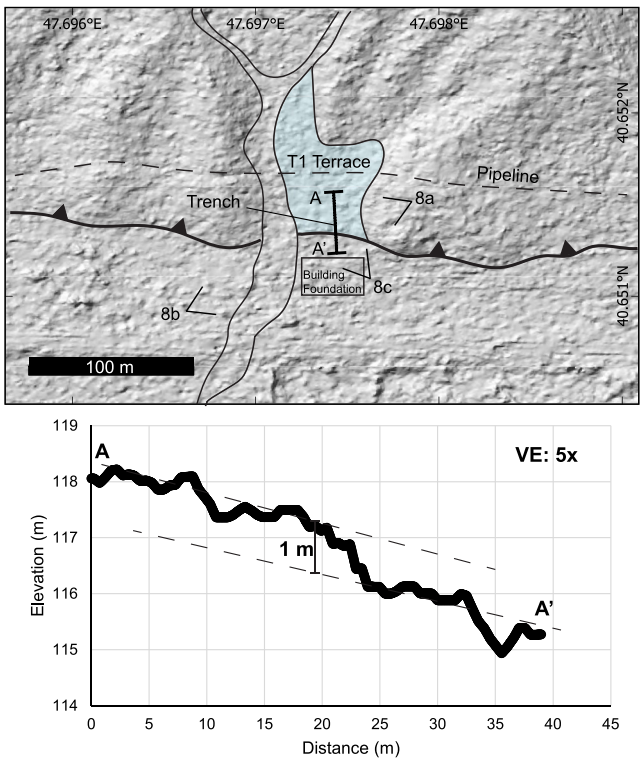

Figure 7. Site map of the Goychay trench site on a hillshade constructed from Pleiades satellite imagery (a) and topographic profile along the path of the trench (b). The trench was excavated across a ~1 m high scarp. Photo locations of Figure 8 indicated on (a).

Near Goychay, the Kura thrust forms a 500 m high rangefront fold scarp comprised of the 2.2–0.88 Ma Unit 1 of Forte et al. (2013) (Figure 1b). Approximately 5 km west of Goychay, a youthful fault scarp can be intermmitently traced for ~1 km. Here, a series of small uplifted hills in front of the main rangefront show a flattening near their front, which we interpret to be evidence of backtilting and active folding. A sharp ~1 m high south-facing fault scarp (Figures 7 and 8) cutting across an alluvial fan forms a small terrace (labeled T1 on Figure 7). The terrace is developed in a small drainage that cuts between these hills (Figure 7). The drainage area is ~5,400 m^2. A field survey of the drainage area shows that it is comprised exclusively of fine-grained primarily silty & clay-rich sediments that are weathered out to form a "badlands" type morphology. The area has extensive anthropogenic modification, and a concrete building foundation was evident immediately adjacent and downslope from the trench site. Uphill and adjacent to the trench site were evident several excavations for gas pipelines and telephone cables. Despite these features, the footprint of the excavated trench (40.651°N, 47.697°E) appeared relatively undisturbed. A drone was not available during the 2023 fieldwork for aerial surveys.

3.3.2. Description of Goychay Trench Exposure

The Goychay trench was 19 m long and 4 m deep. The western wall of the trench was carefully photographed and logged (Figure 9). We did not log the eastern side of the trench because this was benched for trench safety due to the depth of the trench (Figure 9) although we undertook visual comparisons to track units across the trench.The trench revealed a sequence of mostly fine-grained silty/clayey deposits along with several infilled anthropogenic canals, extensive charcoal and pottery layers, and some small lenses comprised of fine gravels and sand. Two low angle north-dipping faults (F1 and F2) displace units within the trench. Most of the unit contacts in the trench are gradational and/or wavy.

The oldest unit in the Goychay trench is U1, a weakly laminated fine-grained clay rich layer found in the hanging wall and footwall of F1, and only the hanging wall of F2. The upper part of U1 contains a 5-10-cm-thick, wavy gray marker horizon that clearly shows evidence of disruption across the two faults. In each fault, this marker horizon warps upward in the hanging walls. Above U1 is U2, a slightly coarser grained and more stratified layer than U1. U2 is found across the entire trench exposure, and while it is only ~1 m thick in the hangingwall of F2, U2 is ~2 m thick in the footwall of F2. In the hangingwall of F2, U2 contains a single 20-cm diameter rounded cobble, and several discontinuous silty/sandy laminae, with a mostly clayey matrix. In the footwall of F2, unit U2 contains several 10–20 cm thick lenses of sand and fine gravel. This forms a sharp contrast with U1 where no lenses of coarser sediment could be found. The upper part of this part of U2 contains numerous scattered rounded cobbles with diameters up to ~20 cm. Capping U2 in the footwalls of faults F1 and F2 is unit U3, which is a fine-grained massive layer primarily comprised of silt and clay.

Above U3 in the hangingwall of fault F2 and capping fault F1 is U4, another fine-grained silty/clay layer. U4 thickens down-slope from F1. Above U4 is U5, which contains abundant 1–2 cm charcoals and pottery fragments. In the lower, southernmost part of the trench, an infilled-canal shaped unit containing mammal bone fragments and several intact clay pots is included as part of U5 based on the similar radiocarbon ages. Above U5 in the hangingwall of F2 is U6, a thin layer, largely devoid of charcoal, and instead containing thin beds of sand and silt. Above U6 is U7, which crosses the entire exposure and is comprised of mostly clays and silts that form a weak blocky structure. U7 also contains disseminated charcoals. In the lower part of the trench toward the south, near the base of the scarp, U8 consists of two infilled canals that have well-defined boundaries. The lower of these canals is basally filled with cobbles, and is infilled with loose gray sand. Plastic trash was found near the base of the higher of these infilled canals, suggesting that they are of modern age. Capping the entire exposure is the modern soil and an anthropogenic trash layer, Unit U9. The very southern edge of the trench revealed part of the

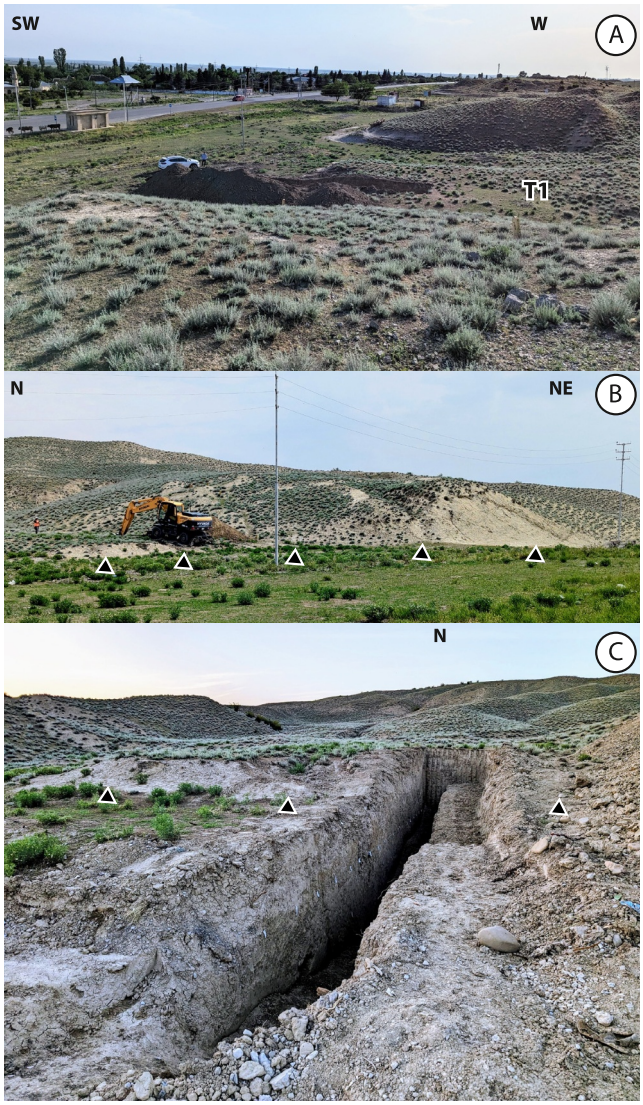

Figure 8. Field photos of the Goychay trench site. Photo locations indicated on Figure 7. Photo (a) shows the T1 terrace that is cut by a scarp. (b) Shows the scarp during excavation and slightly back-tilted hills along the fault. (c) Shows the trench and scarp after excavation.

excavation of the aforementioned concrete building foundation that is adjacent to the trench site, and this is also included in U9.

3.3.3. Goychay Trench Event History

Evidence of faulting in the Goychay trench is most clear based on the truncation and displacement of a light gray horizon at the top of Unit U1 across two faults (F1 and F2; Figure 9), with the older U1 unit overthrusting U2/U3. The light gray layer at the top of U1 is displaced 90 cm across the upper fault, F1. Fault F1 dips to the north at 25°. The light gray layer cannot be found in the footwall of F2, which we interpret here to imply that this layer was faulted below the floor of the trench, which provides a minimum limit of 3.2 m of displacement along fault F2 since the deposition of the top of U1. Thus the summed total displacement of the top of U1 across faults F1 and F2 is a minimum of 4.1 m. In the hangingwall of both faults, this light gray layer warps up along the fault and is subhorizontal in the footwall. Fault F1 is capped by unit U4, providing a clear event horizon for event E1, with the timing restricted between the deposition of units U3 and U4.

We cannot completely rule out that F2 also may have ruptured in a more recent event (E2), which would have broken all of the units U1-U7, and thus postdated the deposition of U7. Our field reconnaissance in this region shows that irrigation canals are very frequently constructed at the base of fault scarps, so the U8 canals may have been constructed at the base of an existing fault scarp. Unfortunately the excavation of these canals obscures any clear evidence for this second event. The displacement of the U2/U3 contact is 1.7 m across fault F2, which would be a total displacement on fault F2 for both the E1 and possible E2 events. Importantly, as U2 is present across the whole trench, we believe that during hanging wall uplift along the two faults, the stratigraphically higher sand and gravel lenses found in the footwall of the lower F2 fault were eroded away from the hangingwall.

3.3.4. Goychay ^{14}C Geochronology

Eight radiocarbon samples in total were analyzed from the Goychay trench. The results and details are listed in Table 1. Six of the samples were charcoals, one was organic sediment (GOY10), and one was a mammal bone (GOY5) found in the southerly part of U3. All of the ages are in stratigraphic order, except for GOY6, which was slightly younger than the other samples from similar layers. The OxCal stratigraphic model (Figure 10) shows that the well defined event, E1 occurred 334-118 BC. If there was a second event, E2 would have occurred sometime in the last 2,000 years.

3.4. Investigation of Damaged Cultural Monuments Near Shamakhi

Three different sites were visited during field mapping in the hanging wall of faults with heavily damaged monuments that predate the 20th Century. Near to Shamakhi, in Mədrəsə (Medrese or Madrasa), a Christian chapel built in 1864 showed extensive damage (Figures 11a–11c). The Mədrəsə Chapel has numerous dropped keystones in arches, cracked walls, and one of the towers had partially collapsed. Also in Shamakhi there were two burial sites with extensive damage to tombs. The Kələxana Tombs (17th Century) had extensive damage to several stone roofs, with roof stones that appeared thrown off (Figure 11e). Likewise, the Yeddi Gumbaz Mausoleum (19th Century), immediately adjacent to the town of Shamakhi, had extensive damage to several of the tombs, including collapsed vaulted roofs (Figure 11d).

10.1029/2023TC007758

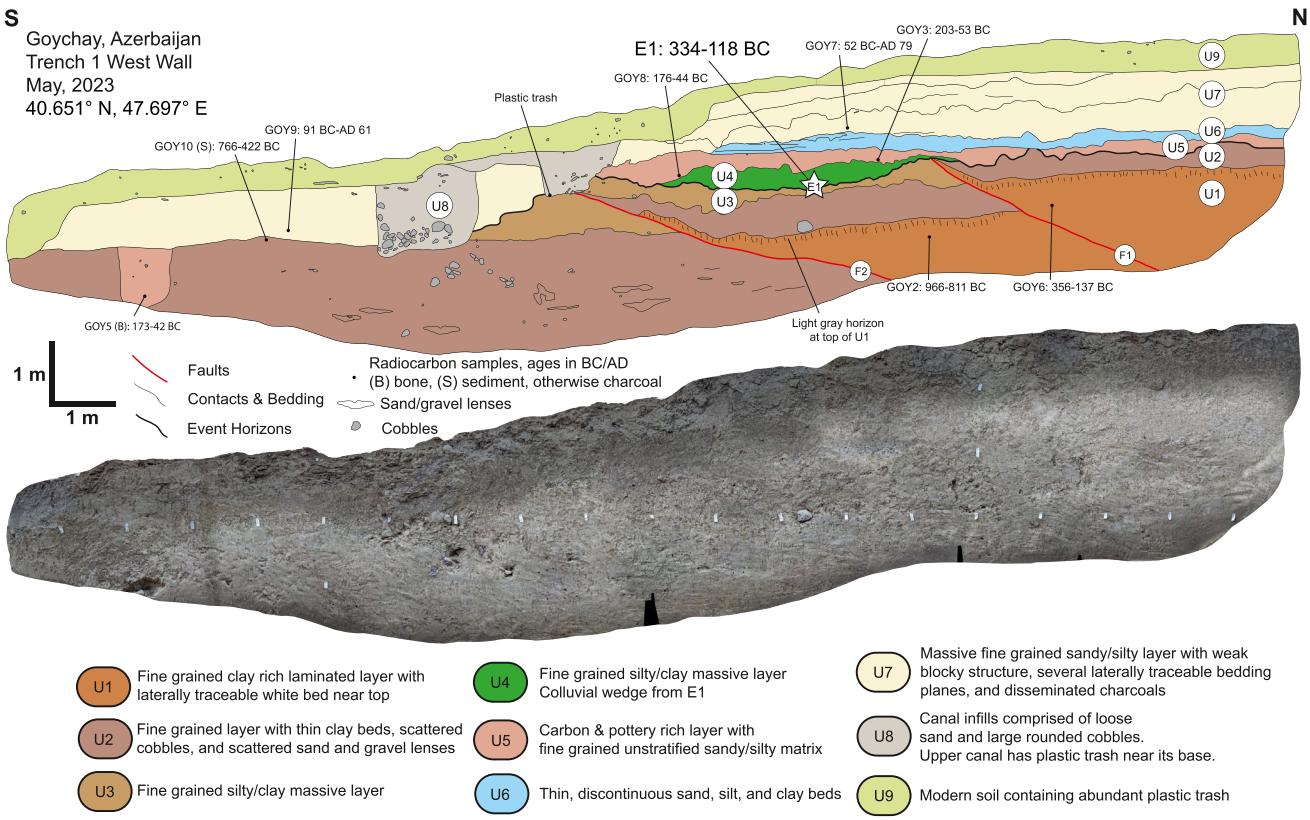

Figure 9. Trench log (upper) and photomosaic (lower) of the west wall of the Goychay trench. Ages listed are modeled ages as described in text. We interpret evidence of one event based on the capping of a clear fault in a narrow light gray horizon at the top of U1. Evidence of possible younger event(s) is obscured by the two infilled canals (U8).

3.5. Slip Rate Measurement Near Garamäyän Ridge

West of Agsu in the foreland is the Garamäyän ridge, a prominent pair of west-northwest-striking active folds that are cut by a series of water gaps (Forte et al., 2013). These folds form the southernmost active fault strand of the Kura fold-thrust belt, and are a different strand than either of the trenched faults. In one of these water gaps ("Gap 2" of Forte et al., 2013) is an inset strath terrace that sits 20 ± 2 m above the modern stream. The southern margin of this terrace is abruptly truncated by an active fault and shows a sharp anticline close to the head of the fault scarp. In a cliff exposure cut for an irrigation canal we found an erosional contact with a strath of subhorizontal fluvial cobbles capping steeply inclined sand and gravel beds (Figure 12). The radiocarbon age dating of a single gastropod shell (WG1, Table 1) (Pigati et al., 2010) sampled from within these horizontal sediments allows for calculation of a vertical uplift rate for this fault. The calibrated age of the shell is 6,975–6,791 cal BP. As shells can contain significant inherited carbon, this should be considered to be the oldest possible age of the deposit. Dividing the 20 m uplift of the terrace (Figure 12b) by this age results in an average vertical uplift rate of 2.9 ± 0.6 mm/yr.

4. Discussion

4.1. Distribution of Slip in the Foreland of the Greater Caucasus

Converting our average of 2.9 mm/yr uplift rate at the water gap site (Figure 12) to dip-slip and shortening-rates requires an assumption of subsurface structural geometry. Forte et al. (2013) model the Garamäyän ridge anticline as a blind fault-propagation fold controlled in the shallowest part by a 20° northeast dipping thrust fault that accommodated 5.6 km of shortening (measured from Fault 8 of Figure 14d in Forte et al., 2013). Our field investigations revealed the presence of surficial fault scarps demonstrating that this fault is not blind. If we assume this 20° dipping thrust fault geometry, and that folding is minimal over the relatively short ~7 Kyr timescale, then

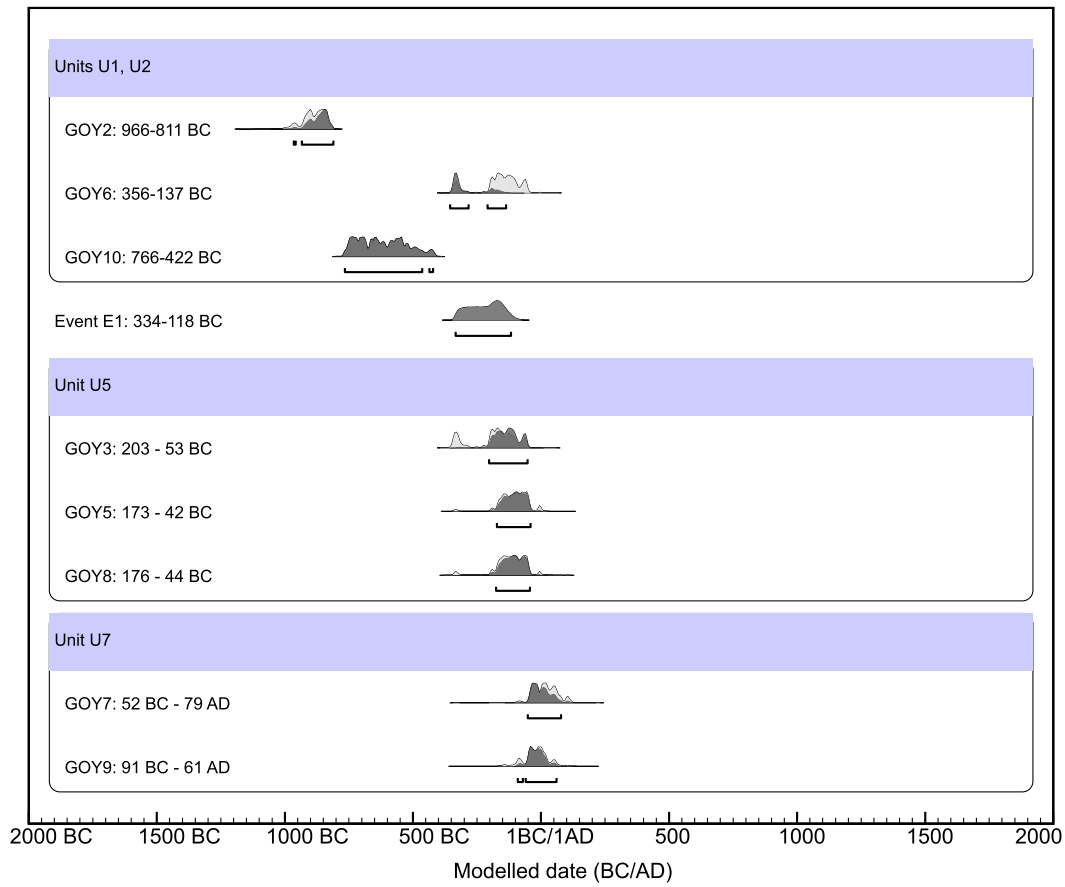

Figure 10. OxCal age model showing radiocarbon ages and event horizons from the Goychay trench. The well constrained E1 event horizon spans 334–118 BC, while a possible later event may have occurred sometime in the last 2,000 years. Dark gray PDF's are the sequence modeled results, while light gray are the full calibrated age ranges.

2.9 mm/yr of uplift corresponds to 8.0 mm/yr of shortening and a dip-slip rate of 8.5 mm/yr. Uncertainties in the geometry and near surface folding processes are significant, but difficult to quantify, and a steeper dipping geometry results in lower dip-slip and shortening rates. Our rates are in-line with the prior structural (6.7–13.6 mm/yr) and geodetic estimates (8–10 mm/yr) across the Kura fold-thrust belt (Forte et al., 2013; Kadirov et al., 2012). However, as our rate was determined from only one of the two main active parallel structures at this longitude (the other was trenched in this study), and this rate consumes nearly all of the budget of the prior estimates, we expect that this rate is thus an upper limit. Regardless, our new rates are consistent with that of Forte et al. (2013), which demonstrates that a significant portion (~80–100%) of both the post-1.5 Ma and present-day geodetic strain budget across the Greater Caucasus is accommodated by the Kura thrust belt.

4.2. Historical Earthquakes

While the Eastern Caucasus have not experienced any $M > 7$ earthquakes during the instrumental period (Telesca et al., 2018; Yetirmishli et al., 2021), the region has experienced numerous pre-instrumental devastating earthquakes, the largest ($M \sim 7$) occurring in AD 1139, 1668, and 1902 (Ismail-Zadeh et al., 2020). The widely felt 1668 and 1902 earthquakes both destroyed the medieval capital city of Shamakhi (Figure 1), while moderate ($M \sim 6$) events in 1828, 1859, 1869, and 1872 caused severe damage to the city.

The 1139 earthquake is reported to have destroyed the city of Ganja in the southwestern part of the Kura basin (Figure 1a). It is unclear whether this event is associated with the Kura fold-thrust belt, or if it occurred in the Lesser Caucasus. However, the AD 1139 earthquake is the earliest earthquake record from the Kura region, and as the region has been continuously inhabited since then, we assume that all significant large earthquakes since that time have been reported.

10.1029/2023TC007758

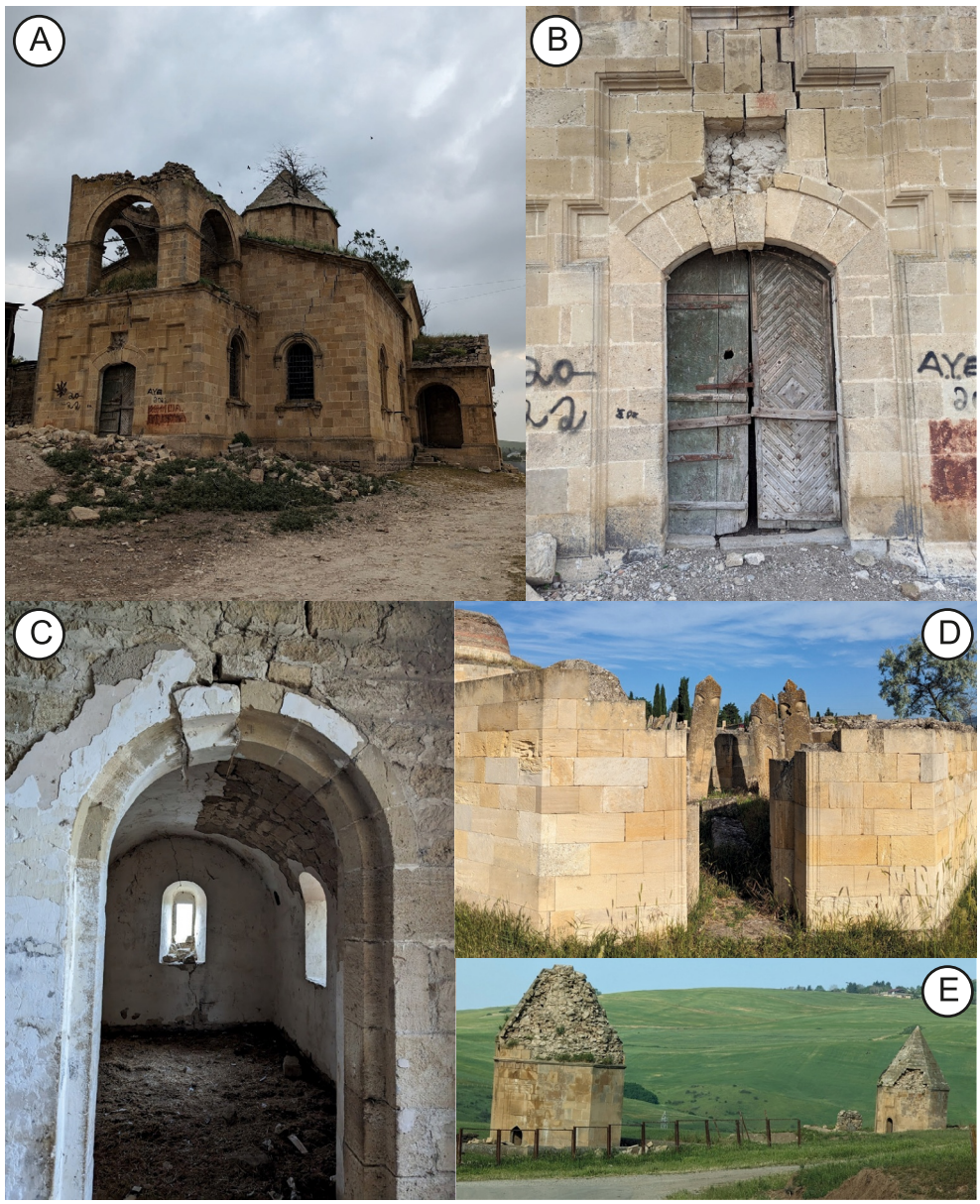

Figure 11. Photos of damaged cultural monuments near Shamakhi (locations on Figure 1B). (a–c) are of the chapel in Medrese (40.610°N, 48.561°E), built in 1864 and reported by Weber (1903) as damaged in the 1902 earthquake. (b, c) show examples of dropped keystones. (d, e) are mausoleums with destroyed (D 40.620°N, 48.635°E) and damaged (E 40.589°N, 48.601°E) roofs, also interpreted here to be from the 1902 earthquake.

A fair amount of detail can be gleaned about the 1668 Shamakhi earthquake from contemporary historical sources (reported dates range from 1667 to 1669). Some of the most widely cited accounts of the damage in Western studies come from European travelers passing through the region around this period. The well-known French traveler, John Tavernier, was in the region during the earthquake but only heard news of the event while in Tabriz. According to the account he received the entire city was demolished and only a handful of people survived (Tavernier, 1678). Somewhat later, Cornelius de Bruijn (translated into English as "Cornelius le Brun") visited Shamakhi, and mentioned that the earthquake, which occurred 35 years before his travels in 1703, destroyed all of the city walls and major monuments including the congregational mosque (Le Brun, 1759). It would appear, however, that the administrative function of the city remained and he mentions smaller mosques and houses that he saw when visiting. The impact on the people was severe enough that a tremor during his visit (1703) saw people flee the city but there was limited or no damage to structures. It is worth noting that de Bruijn's dating

10.1029/2023TC007758

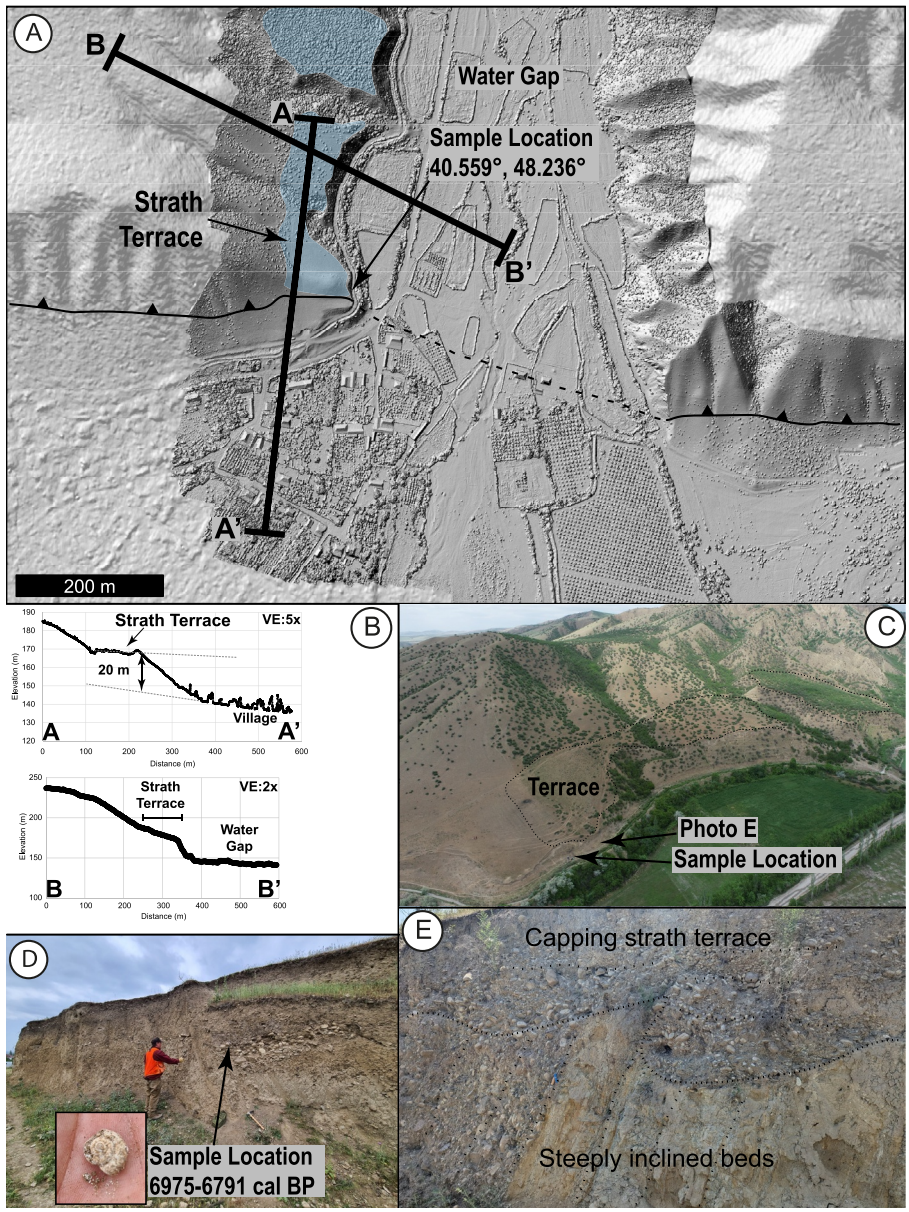

Figure 12. Hillshade image of photogrammetry-derived DEM (a) showing the uplifted strath terrace inset to the watergap (40.559°N, 48.236°E). Profile A-A′ shown in (b) shows 20 m of uplift. B-B′ profile shows relation of strath terrace to higher surface and water gap, also in (b). Oblique aerial photograph of the terrace (c). A gastropod shell (inset) was sampled from subhorizontal fluvial cobbles in an exposure of the strath (d). Photo showing the strath terrace capping steeply dipping Quaternary beds (e).

places this event in 1668, a date accepted by Nikonov in his comprehensive review of the source materials for this earthquake, more specifically he estimates, on the 14th January (Nikonov, 1982). In his chronological table of events, he notes a number of aftershocks ranging from later in 1668, until early 1671. Specific impacts listed by Nikonov based on his assessment of all sources available to him include: destruction of the entire city, between 6,000–8,000 deceased, large numbers of collapsed individual buildings including the city walls and fortress, and landslides causing loss of life (Nikonov, 1982). Sources collated in this work detailing other settlements in the region mention impacts as far away as Baku (a collapsed wall of a palace), detection but no damage in Derbent, and the event was apparently not felt in the more distant heavily populated regions of Tbilisi or Yerevan. Based on the collective data, Nikonov assesses the area of highest impact of the earthquake as IX on the MSK-64 intensity scale in the region of Shamakhi. An inscribed stone in the village of Khnov, near Mishlesh in Dagestan describes

the effects of an earthquake that occurred at roughly the same time (Zakariyaev (Закарияев), 2018). If this is the same earthquake as that felt in Shamakhi, then it is possible that this earthquake ruptured >150 km of the Main Caucasus thrust.

The 1828 Shamakhi event destroyed 526 buildings across the region. The 1859 event killed 100 people, and destroyed 741 buildings, prompting the capital to be relocated from Shamakhi to Baku. The 1872 event killed 118 people and destroyed all but 20 buildings (Shebalin et al., 1982). The 1902 event killed 2,000 people and destroyed 4,000 homes (New York Times, 1902).

In Figure 1b we converted the isoseismals for the 1902 Shamakhi earthquake originally reported in an intensity scale developed by Weber (1903) into the MMI (Modified Mercalli Intensity) scale (Wood & Neumann, 1931). Weber (1903) constructed these isoseismals using observations from 120 villages throughout the region. These isoseismals suggest that the epicenter was close to Shamakhi and that the fault that ruptured follows the overall strike of the Kura thrust.

Our paleoseismic trench results in Agsu provide evidence of two surface rupturing events since the early 18th century (E1: AD 1713–1895 and E2: AD 1872–2003). The younger of these rupturing events, E2, may be the surface rupture of the 1902 Shamakhi earthquake, while the penultimate E1 event could be the 1668 earthquake if we reject two radiocarbon ages (R24 and R29). Present-day Shamakhi is only ∼18 km to the northeast on the hangingwall of the Agsu trench site, and would have experienced high intensity ground motions if the northeast-dipping fault ruptured, so the destruction reported during these events is consistent with our paleoseismic results.

The past magnitude estimate of $M \sim 7$ for the 1902 E2 event from the Agsu trench is reasonable based on comparisons of the 3.5 m displacement in the trench to displacements of other surface rupturing reverse mechanism earthquakes (e.g., Wesnousky, 2008), though such comparisons could be of limited utility due to the paucity of examples of thrust/reverse surface rupturing earthquakes. Based on the larger observed fault slip, E1 from the Agsu trench may have had a larger magnitude than E2. If we assume that the 1902 rupture plane (E2) has dimensions similar to the reported high damage isoseismals (50 × 30 km; Weber, 1903) and slipped an average of 3.5 m (measured from the trench), then using the equation relating moment magnitude to seismogenic moment, where l = rupture length (50 km), w = rupture width (30 km), and d = displacement (3.5 m) (Hanks & Kanamori, 1979, adapted for dyne-cm), the result is an estimated M_w 7.4, much higher than the past estimate of M6.9 from intensity data for the 1902 Shamakhi earthquake. This discrepancy is expected as estimates of magnitude that rely purely on intensity data frequently have uncertainties on the order of a full magnitude unit (Lucas et al., 2023).

The lack of reported historical earthquakes farther to the west in the Kura fold-thrust belt (i.e., near Goychay and west) contrasts with the numerous earthquakes reported near Shamakhi over the past 4 centuries. This lack of reported earthquakes in the western and central Kura fold-thrust belt could be a result of either (a) large earthquakes that are missing from the historical records (due to sparse populations, lapses in record keeping, or other reasons), (b) aseismic deformation (e.g., fault creep), or (c) unreleased moment accumulated in the thrust system. Like prior authors (Jackson & Ambraseys, 1997), we expect that most large (e.g., Mw > 7) earthquakes would have been felt over a wide area and likely would have been recorded, as the aforementioned earthquakes dating back to the 12th Century have been. Given the numerous fault scarps identified during fieldwork and based on our trenching results, we suggest that the fault system does periodically produce surface rupturing earthquakes. Here we assume three possible dates for the last major surface rupturing earthquake along the Kura thrust to the west of Agsu: (a) E1 from the Goychay trench, 334–118 BC; (b) 1139 AD, the Ganja earthquake, which may be mislocated in historical records, as a large subduction event along the Kura fold-thrust would likely have caused destruction in Ganja; or (c) the 1668 Shamakhi earthquake, which caused destruction over a very large area. We did not find either the 1139 or 1668 AD earthquakes in the trench at Goychay, but cannot rule out that these did not rupture a parallel fault strand closer to the Main Caucasus at this latitude or that their evidence was obscured in the trench.

If we assume that strain has accumulated at a rate of ∼10 mm/yr since each of these possible releasing dates, then the Kura fold-thrust belt could have ∼3.5–20.0 m of stored strain in the last 350–2,000 years. The Kura fold-thrust belt soles into a 5° north-dipping detachment at a depth of ∼5 km (Forte et al., 2013), and the minimum width of the thrust belt is ∼25 km, though it should be noted that the base of the seismogenic zone extends to at least a depth of 60 km below the Greater Caucasus (Gunnels et al., 2021; Yetirmishli et al., 2021). Based on this geometry

(width, w = 25 km, length, l = 150–250 km, displacement, d = 3.5–20), we can estimate a magnitude, were the whole fault to rupture, using the above equation. The result demonstrates that the Kura fold-thrust belt could have sufficient stored strain to produce either a single Mw 7.7–8+ earthquake. The subduction zone width is much greater than 25 km (Gunnels et al., 2021), so even larger earthquakes could be anticipated. Alternatively, this strain could be released during a period of time with numerous moderate ($M \sim 7$) earthquakes, or possibly by fault creep. Either scenario represents a significant hazard to the populations and infrastructure of the region, including the large earthen dam and 15,730 km^3 reservoir at Mingecevir built immediately atop the Kura thrust (Figure 1). Fault rupture impacting major critial infrastructure including water and hydrocarbon pipelines, which oftentimes are found at the base of the rangefront, coincident with the faults documented here, will also be of concern.

The contrast in earthquake histories between the central Kura fold-thrust belt and the eastern region near Shamakhi suggests that perhaps ruptures to the west are less frequent but could be significantly larger, while the Shamakhi region (Figure 1) is affected by more frequent moderate ruptures. More paleoseismic trenching, detailed mapping, and dating will be required to confirm our results, ascertain the size of past ruptures in the Kura fold-thrust belt and to investigate how these ruptures are partitioned among the different thrust sheets.

4.3. Archaeoseismology

Fieldwork and assessments of cultural monuments in the research area (a church and tombs) show two primary effects on the built environment from strong ground motions, in particular, dropped key stones in arches of doorways of a church, collapsed vaults, and collapsed and damaged stone walls. Dropped keystones refers to the center of the arch in doorways or windows and are common in areas that experienced strong ground motions during earthquakes (Marco, 2008; Rodríguez-Pascua et al., 2011; Silva et al., 2009). Field observations coupled with finite element modeling show that only major earthquakes cause the downward sliding of arch keystones and thus these dropped keystones are archaeoseismic evidence for a large earthquake greater than Mw 6.5 (Kamai & Hatzor, 2008). It should be noted that other causes can produce structural damage in arches, related to poor foundations of the arch and or relative sliding, however dropped keystones are strong indications of off-fault strong ground motions (e.g., Rodriguez-Pascua et al., 2011). Thus the presence of dropstones (Figure 1b) in the hangingwall of the Kura thrust, suggests the occurrence of shaking that could be attributed to Mw > 6.5 event(s).

Additionally, collapsed walls or vaults are important indications of strong ground motions (e.g., Rodriguez-Pascua et al., 2011), and we visited 2 sites (Figures 11d and 11e) where there are a number of pre-20th century tombs, and some of these have collapsed vaults of the tombs, and roofs that appear to have experienced high accelerations (Figure 11d).

Viewed together, the dropped keystones in the chapel arches and the collapsed vaults of the tombs that are found within 12 km from the Agsu trench site, respectively, and in the hanging wall of the fault provide important off-fault shaking proxies. The damage to the Mədrəsə Chapel was reported by Weber (1903) as a result of the 1902 Shamakhi earthquake. These observations of damage to cultural monuments, observed more than 120 years after the earthquake, provide important data points that demonstrate the effects of destructive earthquakes and are useful archaeoseismology observations for understanding the regional earthquake histories.

5. Conclusions

The two surface rupturing events (AD 1713–1895 and AD 1872–2003) from the Agsu trench are likely the surface ruptures of the Kura Fold and Thrust belt from the historical 1668 and 1902 earthquakes that destroyed the major city and former capital of Azerbaijan, Shamakhi. We reassess the estimated magnitude for the 1902 event and suggest that it could be as large as a Mw 7.4 rather than M 6.9 earthquake. Investigations of historical cultural monuments that were damaged in the 1902 earthquake near Shamakhi, in the hangingwall of the Agsu trench site, provide useful data points for other archaeoseismic studies. The second trench, near Goychay, about 60 km to the west of the Agsu site, revealed evidence of one surface rupturing earthquake from 334 to 118 BC and possibly another more recent event in the last 2,000 years. Further field investigations are required to confirm these results, to place limits on the possible rupture lengths, to better estimate the magnitude of these historical events, and to determine the rupture histories of the other faults in the Kura fold-thrust belt. Dating of an abandoned strath terrace in a water gap on a different fault between the two trench sites provides a maximum limit of ~8 mm/yr of shortening during the Holocene across the youngest active fold west of Agsu. These results are consistent with

Quaternary rates determined from stratigraphic and geodetic studies that yield shortening rates of 6.7–13.6 mm/yr (e.g., Forte et al., 2013; Kadirov et al., 2012), and further demonstrate that most of the convergence between the Arabian plate and Eurasia in the eastern Greater Caucasus is accommodated by the Kura fold-thrust belt (Forte et al., 2013; Kangarli et al., 2018; Mosar et al., 2010). Based on these rates, and if there have been no ruptures of the central and western parts of the Kura fold-thrust system since the last reported historical event in 1668 AD (or earlier), then the system could have sufficient strain accumulated to produce a $M > 7.7$ earthquake with important implications in terms of strong ground motions in the area as well as surface rupture impacts on built infrastructure.

Conflict of Interest

The authors declare no conflicts of interest relevant to this study.

Data Availability Statement

Drone photogrammetry models produced during this study are freely available on OpenTopography.org: https://doi.org/10.5069/G93776XH. Point clouds constructed from Pleiades stereo satellite images are also freely available on OpenTopography.org: https://doi.org/10.5069/G9RJ4GPJ. Photomosaics of paleoseismic trenches are freely available here: https://doi.org/10.5281/zenodo.10407412. All other data used is publicly available or provided in this manuscript.

Acknowledgments
This research was supported in part by the Leverhulme Trust projects "EROICA" (RPG-2018-371) and "NEPTUNE" (RPG-2018-243), by the NERC-ESRC Increasing Resilience to Natural Hazards program "Earthquakes without Frontiers" (NE/J02001X/1), the NERC-funded COMET (GA/13/M/031) and allocation 0009090 from the Research England GCRF support fund. The research was also supported by an Institute of Earth Sciences of the University of Iceland start up grant as well as laboratory support from a University of Iceland Research Fund Grant to GDP. The authors are grateful for field assistance from Sarvat Gurbanzada, Rashid Khalilov, Aslan Sadikov, Telman Jaferov, Rasul Feyzullayev, and Samandar Mammadov. Thanks to Arzu Javadova (SOCAR) and Nazim Abdullayev (BP) for both their scientific input and for helping to organize funding from BP for field and laboratory expenses. Thanks to editor Taylor Schildgen, reviewer Christoph Grützner, and one anonymous reviewer for the thoughtful feedback and discussions that greatly improved this work.

References

Alania, V. M., Chabukiani, A. O., Chagelishvili, R. L., Enukidze, O. V., Gogrichiani, K. O., Razmadze, A. N., & Tsereteli, N. S. (2017). Growth structures, piggy-back basins and growth strata of the Georgian part of the Kura foreland fold–thrust belt: Implications for Late Alpine kinematic evolution. *Geological Society, London, Special Publications*, *428*(1), 171–185. https://doi.org/10.1144/SP428.5

Allen, M. B., Vincent, S. J., Alsop, G. I., Ismail-zadeh, A., & Flecker, R. (2003). Late Cenozoic deformation in the South Caspian region: Effects of a rigid basement block within a collision zone. *Tectonophysics*, *366*(3–4), 223–239. https://doi.org/10.1016/S0040-1951(03)00098-2

Andrews, D. J., & Hanks, T. C. (1985). Scarp degraded by linear diffusion: Inverse solution for age. *Journal of Geophysical Research*, *90*(B12), 10193–10208. https://doi.org/10.1029/jb090ib12p10193

Avdeev, B., & Niemi, N. A. (2011). Rapid Pliocene exhumation of the central Greater Caucasus constrained by low-temperature thermochronometry. *Tectonics*, *30*(2), TC2009. https://doi.org/10.1029/2010TC002808

Bronk Ramsey, C. (1995). Radiocarbon calibration and analysis of stratigraphy: The OxCal program. *Radiocarbon*, *37*(2), 425–430. https://doi.org/10.1017/S0033822200030903

Cowgill, E., Forte, A. M., Niemi, N., Avdeev, B., Tye, A., Trexler, C., et al. (2016). Relict basin closure and crustal shortening budgets during continental collision: An example from Caucasus sediment provenance. *Tectonics*, *35*(12), 2918–2947. https://doi.org/10.1002/2016TC004295

Dziewonski, A. M., Chou, T.-A., & Woodhouse, J. H. (1981). Determination of earthquake source parameters from waveform data for studies of global and regional seismicity. *Journal of Geophysical Research*, *86*(B4), 2825–2852. https://doi.org/10.1029/JB086iB04p02825

Ekström, G., Nettles, M., & Dziewoński, A. M. (2012). The global CMT project 2004–2010: Centroid-moment tensors for 13,017 earthquakes. *Physics of the Earth and Planetary Interiors*, *200–201*, 1–9. https://doi.org/10.1016/j.pepi.2012.04.002

Engdahl, E. R., Di Giacomo, D., Sakarya, B., Gkarlaouni, C. G., Harris, J., & Storchak, D. A. (2020). ISC-EHB 1964-2016, an improved data set for studies of Earth structure and global seismicity. *Earth and Space Science*, *7*(1), e2019EA000897. https://doi.org/10.1029/2019ea000897

Engdahl, E. R., van der Hilst, R., & Buland, R. (1998). Global teleseismic earthquake relocation with improved travel times and procedures for depth determination. *Bulletin of the Seismological Society of America*, *88*(3), 722–743. https://doi.org/10.1785/BSSA08800307222

Forte, A. M. (2012). Late Cenozoic evolution of the Greater Caucasus Mountains and Kura foreland basin: Implications for early orogenesis. (Ph. D.). University of California.

Forte, A. M., Cowgill, E., Bernardin, T., Kreylos, O., & Hamann, B. (2010). Late Cenozoic deformation of the Kura fold-thrust belt, southern Greater Caucasus. *Bulletin of the Geological Society of America*, *122*(3–4), 465–486. https://doi.org/10.1130/B26464.1

Forte, A. M., Cowgill, E., Murtuzayev, I., Kangarli, T., & Stoica, M. (2013). Structural geometries and magnitude of shortening in the eastern Kura fold-thrust belt, Azerbaijan: Implications for the development of the Greater Caucasus Mountains. *Tectonics*, *32*(3), 688–717. https://doi.org/10.1002/tect.20032

Forte, A. M., Cowgill, E., & Whipple, K. X. (2014). Transition from a singly vergent to doubly vergent wedge in a young orogen: The Greater Caucasus. *Tectonics*, *33*(11), 2077–2101. https://doi.org/10.1002/2014TC003651

Forte, A. M., Whipple, K. X., & Cowgill, E. (2015). Drainage network reveals patterns and history of active deformation in the eastern Greater Caucasus. *Geosphere*, *11*(5), 1343–1364. https://doi.org/10.1130/GES01121.1

Grützner, C., Schneiderwind, S., Papanikolaou, I., Deligiannakis, G., Pallikarakis, A., & Reicherter, K. (2016). New constraints on extensional tectonics and seismic hazard in northern Attica, Greece: The case of the Milesi Fault. *Geophysical Journal International*, *204*(1), 180–199. https://doi.org/10.1093/gji/ggv443

Gunnels, M., Yetrimishli, G., Kazimova, S., & Sandvol, E. (2021). Seismotectonic evidence for subduction beneath the eastern Greater Caucasus. *Geophysical Journal International*, *224*(3), 1825–1834. https://doi.org/10.1093/gji/ggaa522

Hanks, T. C., & Kanamori, H. (1979). A moment magnitude scale. *Journal of Geophysical Research*, *84*(B5), 2348–2350. https://doi.org/10.1029/JB084iB05p02348

International Seismological Centre. (2022). ISC-EHB dataset. https://doi.org/10.31905/PY08W6S3

Ismail-Zadeh, A., Adamia, S., Chabukiani, A., Chelidze, T., Cloetingh, S., Floyd, M., et al. (2020). Geodynamics, seismicity, and seismic hazards of the Caucasus. *Earth-Science Reviews*, *207*, 103222. https://doi.org/10.1016/j.earscirev.2020.103222

Jackson, J., Priestley, K., Allen, M., & Berberian, M. (2002). Active tectonics of the South Caspian basin. *Geophysical Journal International*, *148*(2), 214–245. https://doi.org/10.1046/j.1365-246X.2002.01005.x

Jackson, J. A., & Ambraseys, N. N. (1997). Convergence between Eurasia and Arabia in eastern Turkey and the Caucasus. *Historical and Prehistorical Earthquakes in the Caucasus*, *28*, 79–90. https://doi.org/10.1007/978-94-011-5464-2_3

Kadirov, F., Floyd, M., Alizadeh, A., Guliev, I., Reilinger, R., Kuleli, S., et al. (2012). Kinematics of the eastern Caucasus near Baku, Azerbaijan. *Natural Hazards*, *63*(2), 997–1006. https://doi.org/10.1007/s11069-012-0199-0

Kamai, R., & Hatzor, Y. H. (2008). Numerical analysis of block stone displacements in ancient masonry structures: A new method to estimate historic ground motions. *International Journal for Numerical and Analytical Methods in Geomechanics*, *32*(11), 1321–1340. https://doi.org/10.1002/nag.671

Kangarli, T. N., Kadirov, F. A., Etirmishli, G. D., Aliev, F. A., Kazimova, S. E., Aliev, A. M., et al. (2018). Geodynamics, active faults and earthquake source mechanisms in the zone of pseudosubduction interaction of continental microplates in the South and North Caucasus (southern slope of the Greater Caucasus, Azerbaijan). *Geodynamics and Tectonophysics*, *9*(4), 1099–1126. https://doi.org/10.5800/GT-2018-9-4-0385

Le Brun, C. (1759). *A new and more correct translation than has Hitherto appeared in public of Mr. Cornelius Le Brun's travels into Moscovy, Persia, and divers parts of the East-Indies; containing an accurate description of all such articles as are most remarkable in each of those different countries, and most worthy the attention of the curious reader. As also of their antiquities; but more particularly those relating to the famous palace of Persepolis, commonly called Chelminar by the Persians: By a gentleman of Oxford*. J. Warcus.

Lucas, M. C., Hough, S. E., Stein, S., Salditch, L., Gallahue, M. M., Neely, J. S., & Abrahamson, N. (2023). Uncertainties in intensity-based earthquake magnitude estimates. *Seismological Research Letters*, *94*(5), 2202–2214. https://doi.org/10.1785/0220230030

Marco, S. (2008). Recognition of earthquake-related damage in archaeological sites: Examples from the Dead Sea fault zone. *Tectonophysics, Earthquake Geology: Methods and Applications*, *453*(1–4), 148–156. https://doi.org/10.1016/j.tecto.2007.04.011

McCalpin, J. (2009). *Paleoseismology* (2nd ed.). Academic Press.

McKenzie, D. (1972). Active tectonics of the Mediterranean region. *Geophysical Journal International*, *30*(2), 109–185. https://doi.org/10.1111/j.1365-246X.1972.tb02351.x

Mosar, J., Kangarli, T., Bochud, M., Glasmacher, U. A., Rast, A., Brunet, M.-F., & Sosson, M. (2010). Cenozoic-recent tectonics and uplift in the Greater Caucasus: A perspective from Azerbaijan. *Geological Society, London, Special Publications*, *340*(1), 261–280. https://doi.org/10.1144/SP340.12

Mumladze, T., Forte, A. M., Cowgill, E. S., Trexler, C. C., Niemi, N. A., Burak Yıkılmaz, M., & Kellogg, L. H. (2015). Subducted, detached, and torn slabs beneath the Greater Caucasus. *GeoResJ*, *5*, 36–46. https://doi.org/10.1016/j.grj.2014.09.004

New York Times, T. (1902). 2,000 dead at shemakha. *New York Times*, *1*.

Nikonov, A. A. (1982). Sil'neĭshee Zemletriasenie Bol'shogo Kavkaza 14 Ianvaria 1668 g. Fis. Zemli. (Vol. *9*, pp. 90–106).

Ovsyuchenko, A. N., Marakhanov, A. V., Lar'kov, A. S., & Novikov, S. S. (2014). Late quaternary dislocations and seismotectonics of the Racha earthquake source, the Greater Caucasus. *Geotectonics*, *48*(6), 440–458. https://doi.org/10.1134/S0016852114050057

Philip, H., Cisternas, A., Gvishiani, A., & Gorshkov, A. (1989). The Caucasus: An actual example of the initial stages of continental collision. *Tectonophysics*, *161*(1–2), 1–21. https://doi.org/10.1016/0040-1951(89)90297-7

Philip, H., Rogozhin, E., Cisternas, A., Bousquet, J. C., Borisov, B., & Karakhanian, A. (1992). The Armenian earthquake of 1988 December 7: Faulting and folding, neotectonics and palaeoseismicity. *Geophysical Journal International*, *110*(1), 141–158. https://doi.org/10.1111/j.1365-246X.1992.tb00718.x

Pierce, I. (2022). Surveys of Kura frontal thrust, Azerbaijan, 2022 [Dataset]. Open Topography. https://doi.org/10.5069/G93776XH

Pierce, I. (2023). Photomosaics of paleoseismic trenches in Azerbaijan [Dataset]. Zenodo. https://doi.org/10.5281/zenodo.10407412

Pierce, I., & Koehler, R. (2023). 3D Paleoseismology from iOS lidar and structure from motion photogrammetry: A case study on the Dog Valley fault, California. *Seismica*, *2*(1). https://doi.org/10.26443/seismica.v2i1.208

Pierce, I., & Walker, R. (2023). Satellite derived point clouds of the Kura thrust belt, Shamakhi, Azerbaijan, 2021. [Dataset]. Open Topography. https://doi.org/10.5069/G9RJ4GPJ

Pigati, J. S., Rech, J. A., & Nekola, J. C. (2010). Radiocarbon dating of small terrestrial gastropod shells in North America. *Quaternary Geochronology*, *5*, 519–532. https://doi.org/10.1016/j.quageo.2010.01.001

Reilinger, R., McClusky, S., Vernant, P., Lawrence, S., Ergintav, S., Cakmak, R., et al. (2006). GPS constraints on continental deformation in the Africa-Arabia-Eurasia continental collision zone and implications for the dynamics of plate interactions. *Journal of Geophysical Research*, *111*(B5), B05411. https://doi.org/10.1029/2005JB004051

Rodríguez-Pascua, M. A., Pérez-López, R., Giner-Robles, J. L., Silva, P. G., Garduño-Monroy, V. H., & Reicherter, K. (2011). A comprehensive classification of Earthquake Archaeological Effects (EAE) in archaeoseismology: Application to ancient remains of Roman and Mesoamerican cultures. *Quaternary International* S1040618211002643. https://doi.org/10.1016/j.quaint.2011.04.044

Rogozhin, E. A., Marakhanov, A. V., Ovsyuchenko, A. N., Spiridonov, A. V., Burkanov, E. E., & Gurbanov, A. G. (2004). Ancient earthquake dislocations in the area of Elbrus Volcano, North Caucasus. *Russian Journal of Earth Sciences*, *6*(4), 293–309. https://doi.org/10.2205/2004ES000160

Shebalin, N. V., Kondorskaia, N. V., & World Data Center A for Solid Earth Geophysics (1982). *New catalog of strong earthquakes in the U.S.S.R. from ancient times through 1977, report SE;31*. World Data Center A for Solid Earth Geophysics.

Silva, P. G., Reicherter, K., Grützner, C., Bardají, T., Lario, J., Goy, J. L., et al. (2009). Surface and subsurface palaeoseismic records at the ancient Roman city of Baelo Claudia and the Bolonia Bay area, Cádiz (south Spain). *Geological Society, London, Special Publications*, *316*(1), 93–121. https://doi.org/10.1144/SP316.6

Sokhadze, G., Floyd, M., Godoladze, T., King, R., Cowgill, E. S., Javakhishvili, Z., et al. (2018). Active convergence between the Lesser and Greater Caucasus in Georgia: Constraints on the tectonic evolution of the Lesser–Greater Caucasus continental collision. *Earth and Planetary Science Letters*, *481*, 154–161. https://doi.org/10.1016/j.epsl.2017.10.007

Stahl, T. A., Cowgill, E., Boichenko, G., Vasey, D. A., & Godoladze, T. (2022). Recent surface rupturing earthquakes along the South Flank of the Greater Caucasus near Tbilisi, Georgia. *Bulletin of the Seismological Society of America*, *112*(4), 2170–2188. https://doi.org/10.1785/0120210267

Sukhishvili, L., Forte, A. M., Merebashvili, G., Leonard, J., Whipple, K. X., Javakhishvili, Z., et al. (2021). Active deformation and Plio-Pleistocene fluvial reorganization of the western Kura fold–thrust belt, Georgia: Implications for the evolution of the Greater Caucasus Mountains. *Geological Magazine*, *158*(4), 583–597. https://doi.org/10.1017/S0016756820000709

Tavernier, J.-B. (1678). *The six voyages of John Baptista Tavernier, a noble man of France now living, through Turky into Persia and the East-Indies, finished in the year 1670: Giving an account of the state of those countries: Illustrated with divers sculptures; together with a new relation of the present Grand Seignor's Seraglio, by the same author*. John Philips.

Telesca, L., Kadirov, F., Yetirmishli, G., Safarov, R., & Kazimova, S. (2018). Joint use of seismological and topological statistical methods for the analysis of 2010–2016 Azerbaijan seismicity. *Pure and Applied Geophysics*, *175*(12), 4225–4239. https://doi.org/10.1007/s00024-018-1945-3

Tibaldi, A., Alania, V., Bonali, F. L., Enukidze, O., Tsereteli, N., Kvavadze, N., & Varazanashvili, O. (2017). Active inversion tectonics, simple shear folding and back-thrusting at Rioni Basin, Georgia. *Journal of Structural Geology*, *96*, 35–53. https://doi.org/10.1016/j.jsg.2017.01.005

Trexler, C. C., Cowgill, E., Spencer, J. Q. G., & Godoladze, T. (2020). Rate of active shortening across the southern thrust front of the Greater Caucasus in western Georgia from kinematic modeling of folded river terraces above a listric thrust. *Earth and Planetary Science Letters*, *544*, 116362. https://doi.org/10.1016/j.epsl.2020.116362

Triep, E. G., Abers, G. A., Lerner-Lam, A. L., Mishatkin, V., Zakharchenko, N., & Starovoit, O. (1995). Active thrust front of the Greater Caucasus: The April 29, 1991, Racha earthquake sequence and its tectonic implications. *Journal of Geophysical Research*, *100*(B3), 4011–4033. https://doi.org/10.1029/94JB02597

Trifonov, V. G. (1978). Late Quaternary tectonic movements of western and central Asia. *Geological Society of America Bulletin*, *89*(7), 1059. https://doi.org/10.1130/0016-7606(1978)89<1059:LQTMOW>2.0.CO;2

Weber, V. (1903). Shamakhi earthquake of 13 February 1902. In *Proceedings of the St. Petersburg geological committee*.

Wesnousky, S. G. (2008). Displacement and geometrical characteristics of earthquake surface ruptures: Issues and implications for seismic-hazard analysis and the process of earthquake rupture. *Bulletin of the Seismological Society of America*, *98*(4), 1609–1632. https://doi.org/10.1785/0120070111

Weston, J., Engdahl, E. R., Harris, J., Di Giacomo, D., & Storchak, D. A. (2018). ISC-EHB: Reconstruction of a robust earthquake dataset. *Geophysical Journal International*, *214*(1), 474–484. https://doi.org/10.1093/gji/ggy155

Wimpenny, S., & Watson, C. S. (2020). gWFM: A global catalog of moderate-magnitude earthquakes studied using teleseismic body waves. *Seismological Research Letters*, *92*(1), 212–226. https://doi.org/10.1785/0220200218

Wood, H. O., & Neumann, F. (1931). Modified Mercalli intensity scale of 1931. *The Bulletin of the Seismological Society of America*, *21*(4), 277–283. https://doi.org/10.1785/bssa0210040277

Yetirmishli, G. J., Ismayilova, S. S., & Kazimova, S. E. (2021). Seismicity of the territory of Azerbaijan in 2019. *Seismoprognosis Observations in the Territory of Azerbaijan*, *19*, 3–18.

Yetirmishli, G. J., Kazimov, I. E., & Kazimova, A. F. (2022). Analysis of modern movements of Earth crust blocks in Azerbaijan according to the data of GPS stations in 2020-2021. *Seismoprognosis Observations in the Territory of Azerbaijan*, *21*, 19–24.

Zelenin, E., Bachmanov, D., Garipova, S., Trifonov, V., & Kozhurin, A. (2022). The Active Faults of Eurasia Database (AFEAD): The ontology and design behind the continental-scale dataset. *Earth System Science Data*, *14*(10), 4489–4503. https://doi.org/10.5194/essd-14-4489-2022

Zhang, H., Aldana-Jague, E., Clapuyt, F., Wilken, F., Vanacker, V., & Van Oost, K. (2019). Evaluating the potential of post-processing kinematic (PPK) georeferencing for UAV-based structure-from-motion (SfM) photogrammetry and surface change detection. *Earth Surface Dynamics*, *7*(3), 807–827. https://doi.org/10.5194/esurf-7-807-2019

Закарияев Замир Шахбанович. (2018). Арабоязычные надписи XVII–XVIII вв. *Из селения Хнов о строительстве минаретов и м ети*. https://doi.org/10.24411/2618-6772-2018-12005